DESIGN OF HIGH EFFICIENCY $In_xGa_{1-x}N$-BASED MULTIJUNCTION SOLAR CELLS

by

Md. Rafiqul Islam

A thesis
Submitted to the Department of Electrical & Electronic Engineering, Khulna
University of Engineering & Technology (KUET) in Partial Fulfillment of the
Requirements for the Degree of
Master of Science
in
Electrical & Electronic Engineering

November 2006

**Department of Electrical & Electronic Engineering
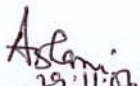Khulna University of Engineering & Technology (KUET)
Khulna-920300**

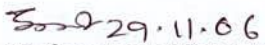# Design of High Efficiency In$_x$Ga$_{1-x}$N-Based Multi-Junction Solar Cells

by

Md. Rafiqul Islam

A Thesis Submitted to the Department of Electrical & Electronic Engineering, Khulna University of Engineering & Technology (KUET) in Partial Fulfillment of the Requirements for the Degree of **Master of Science** in Electrical & Electronic Engineering is Approved.
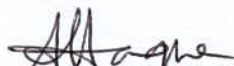
Committee Members

Dr. Ashraful Ghani Bhuiyan Assistant Professor & Supervisor Department of Electrical and Electronic Engineering	Chairman
Professor Dr. Nurunnabi Mollah Head, Department of Electrical and Electronic Engineering	Member
Dr. Md. Rafiqul Islam Associate Professor & co-supervisor Department of Electrical and Electronic Engineering	Member
Professor Dr. B. C. Ghosh Department of Electrical and Electronic Engineering	Member
Mr. A. N. M. Enamul Kabir Associate Professor Department of Electrical and Electronic Engineering	Member
Dr. Anisul Haque Professor and Chairperson Department of Electrical and Electronic Engineering East West University, Dhaka	External Member

Khulna University of Engineering & Technology (KUET)
Khulna-920300, Bangladesh.
November 2006

Declaration

This work has been done by me and it has not been submitted elsewhere the award of any degree or diploma.

Countersigned

29.11.02
(Dr. Ashraful Ghani Bhuiyan)
Supervisor

(Md. Rafiqul Islam)

Acknowledgement

Author

Abstract

Photovoltaic (PV) power generation is becoming widespread as a clean and gentle energy source for the earth. The main drawback of currently used photovoltaic cell is its low conversion efficiency and materials with the appropriate band gaps that can perfectly match the broad range of solar radiation. Recently it has been shown that the energy gap of $In_xGa_{1-x}N$ alloys potentially can be continuously varied from 0.7 to 3.4 eV, providing a perfect matching to the full-solar-spectrum. Therefore, $In_xGa_{1-x}N$ becomes a promising material for very high efficiency multijunction solar cell. Any desired value of bandgap can be obtained from this material choosing the appropriate composition. In this work, $In_xGa_{1-x}N$-based multijunction solar cells have been designed theoretically for high efficiency and the performance of the designed solar cells are evaluated with various parameters. The theoretical design and performance evaluation are done by developing a simulation model. The developed mode optimized the solar cell design for high efficiency at different junction numbers. The efficiency is found to be varied from 24.49 to 45.35 % for single junction to eight junction solar cells. The current mismatches of multijunction solar cell are kept within 0.29%. The lattice mismatches between different cells were found to be varied from 0.86 to 3.15%. The increase in surface recombination velocity and emitter thickness decreases the efficiency. On the other hand, the increase in minority carrier lifetime of emitter and base, and doping density increase the efficiency. In order to get more accurate results the effect of depletion width was taken into account. However, no significant change is observed between the results without and with considering depletion width. The performance of InGaN-based MJ solar cells under concentrator is studied. The efficiency is found to be varied from 24.49 to 39.28 (%) for single junction and 45.35 to 72.79 (%) for eight junction, without and with concentrator, respectively. This model can be applied to design the solar cells at any number of junctions.

Contents

List of Figures

List of Tables

List of Symbols

α	Absorption Coefficient
η	Efficiency of Solar cell
Φ_0	Input Energy
ε	Dielectric constant
AR	Anti-reflection
BSF	Back surface field
D_p	Drift velocity of hole
D_n	Drift velocity of electron
EHP	Electron-hole pair
E_g	Band gap energy
E_0	Built-in potential
e	Charge of an electron
FF	Fill factor of solar cell
F	No of incident photon
H'	Thickness of p-region
I_{mp}	Current in maximum power condition
I_{SC}	Short circuit current
J_{SC}, J_L	Short circuit current density
J_0	Saturation current density
J_{ph}	Photogenerated current
J_p	Photogenerated current in p-region
J_n	Photogenerated current in n-region
J_W	Photogenerated current in depletion region
L_n	Diffusion length of electron
l_n	Length of neutral n-region
L_p	Diffusion length of hole
l_p	Length of neutral p-region
N_A	Acceptor atom concentration

N_D	Donor atom concentration
N_C	Density of states for conduction band
N_V	Density of states for valance band
n_i	Intrinsic carrier concentration
R	Reflection coefficient
S_n	Surface recombination velocity in n-region
S_p	Surface recombination velocity in p-region
SCL	Space charge layer
T	Temperature
t/MWh	Ton per megawatt hour
V_{OC}	Open circuit voltage
V_{mp}	Voltage in maximum power condition
W	Depletion width
X_j	Thickness of n-region
x	Indium composition in $In_xGa_{1-x}N$
ζ	Electric field

CHAPTER *1*

Introduction

1.1 Background Information

Present day civilization and industries are highly dependent on energy. The main sector contributing this huge amount of energy generation is the fossil fuel with limited resources. Some of these resources are only available in few regions of the world; the scarcity also poses a risk to national and regional resource security and autonomy as well as to international security. The difficulty and cost of safety disposing radioactive material and toxic waste, makes the use of nuclear and chemical energy a questionable solution. Also the fossil fuel is costly for transmitting in remote areas. Therefore, renewable sources of energy need to be considered seriously for two main reasons: i) to meet the world-wide energy demand and ii) to protect the environment from the destructive burning of fossil and other fuels.

Renewable energies such as wind power, water, biomass and active and passive solar energy have the potential to overcome these problems, as they are unlimited. Due to the decentralized and distributed nature of most of these energy sources, they provide the energy when and where it is needed and ensure national and regional resource security. The reliability of the power supply from renewable energies is usually higher than from conventional energy sources. The solar energy is the most important renewable source, and convertible into useful form with no transmission cost and environment pollution. Bangladesh is situated closer to equilateral zone and sees solar energy with a good potential throughout the year. Also we have a significant amount of remote areas especially the coastal zone where it is very difficult to erect transmission lines or gas pipes. So, photovoltaic converters may be employed for direct energy conversion in these areas to meet the energy demand of people living there.

At 1839, French physicist Antoine-Cesar Becquerel observed that shining light on an electrode submerged in a conductive solution would create an electric current which introduced the Solar cell technology. Charles Fritts constructed the first true solar cells (at least, the first resembling modern cells in that it was made from only solid materials) by using junctions formed by coating the semiconductor selenium with an ultra thin, nearly transparent layer of gold in 1877. Fritts's devices were very inefficient, transforming less than 1 percent of the absorbed light into electrical energy, but they were a start. Substantial improvements in solar cell efficiency had to wait for a better understanding of the physical principles involved in their design, provided by Einstein in 1905 and Schottky in 1930. By 1927 another metal-semiconductor junction solar cell, in this case made of copper and the semiconductor copper oxide, had been demonstrated. By the 1930s both the selenium cell and the copper oxide cell were being employed in light-sensitive devices, such as photometers, for use in photography. These early solar cells, however, still had energy conversion efficiencies of less than 1 percent (so they made fine light sensors, but lousy energy converters). Solar cell efficiency finally saw substantial progress with the development of the first silicon cell by Russell Ohl in 1941. In 1954,

three other American researchers, G.L. Pearson, Daryl Chapin, and Calvin Fuller, demonstrated a further-refined silicon solar cell capable of 6% energy conversion efficiency (in direct sunlight). By the late 1980s silicon cells, as well as those made of gallium arsenide, with efficiencies of more than 20% had been fabricated. In 1989 a concentrator solar cell, a type of device in which sunlight is concentrated onto the cell surface by means of lenses, achieved an efficiency of 37% thanks to the increased intensity of the collected energy. However, still the efficiency of conventional and commercially available solar cells is very low. Other associated drawbacks, such as optimum power controlling and tracking of the PV array have been solved with the present technology.

Searches for new photovoltaic cells with higher efficiency are being conducted all over the world from the beginning of this decade. Attempts have been made to fabricate photovoltaic cells with materials other than silicon and at the same time modifications in design are being carried out to reduce the reflected component of solar energy. It is evident from the literatures of this field that there are a lot of materials available on high efficiency solar cells. Unfortunately, these cells are in the development stage in the laboratories, and still research is going on to fabricate low cost and high efficiency solar cells with improved performance. Single junction solar cell is not able to convert full spectrum solar energy to electrical energy. If photons have energy exceeding the semiconductor's band gap, the excess is usually dissipated as heat and is thus wasted. Alternatively, photons whose energies are less than the band-gap are not absorbed at all, but are transmitted through the material and their energy is not used. To overcome these difficulties and increase the efficiency of the solar cells multijunction (MJ) approach has been used all over the world. It has been shown that the band gap of $In_xGa_{1-x}N$ alloys can be varied continuously from 0.7 to 3.4 eV by choosing a proper value of composition, which offering a unique opportunity to design MJ solar cells using a single ternary alloy [1].

Concentrator photovoltaic systems using high efficiency solar cells are one of the important issues in the development of an advanced PV system. The production cost of MJ solar cells composed of III–V materials is higher than that of Si solar cells. Replacing semiconductor solar cell area with lower cost plastic lenses leads to lower overall system cost. However, the necessary cell size decreases using concentrator with increasing the efficiency. High-efficiency MJ cells under high concentrations have been investigated for terrestrial applications [2, 3]. Also, for low concentration operation, MJ cells have been investigated for space satellite use [4–6].

1.2   Purpose of Research

To be competitive with the conventional energy source the efficiency of solar cell must be improved. The cost of solar energy must be comparable with the cost of conventional energy. There are many factors which affect the cost of solar energy. The cost of solar energy may be reduced by improving the performance of solar cells. In addition, the concentrator photovoltaic system also reduces the cost of solar cell directly. Among the performance parameters, the efficiency of solar cell is very important. There are many approaches to increase the efficiency, such as MJ solar cells, Multiple spectrum solar cells, Multiple absorption path solar cells, Multiple energy level solar cells, Multiple temperature solar cells. MJ solar cell is the promising approach to increase the efficiency. Currently used MJ solar cells are based on two or three junctions of different semiconductor materials connected in series [7–9]. It has been shown that, theoretically, the efficiency of MJ solar cells increases as it incorporates more and more junctions [10]. However, practically, there is a very little range of materials that could be used to make these cells. The primary requirements for the materials to be used for MJ solar cells are band gap matching with the solar spectrum, high mobilities and lifetimes of charge carriers, thermal and lattice matching, etc. A major challenge in achieving widespread use of these MJ solar cells lies in the identification of materials with the appropriate band gaps. The currently used conventional materials for MJ solar cells are not suitable
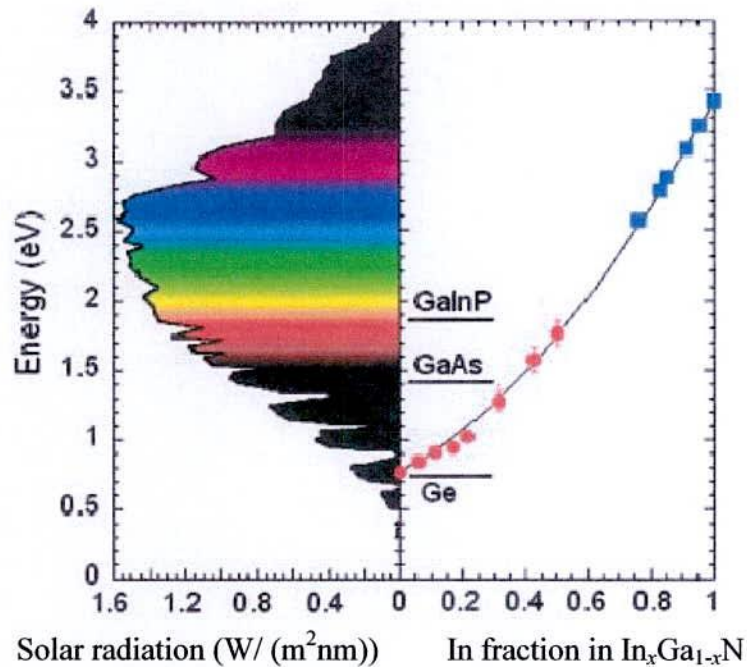
Fig. 1 Band gap energies of the $In_xGa_{1-x}N$ alloy system cover the entire air-mass-1.5 solar spectrum. The gap energies of conventional MJ solar cell materials (Ge, GaAs, and GaInP) are also shown in the right hand panel for comparison (Ref. 1).

according to the requirements. Recently, $In_xGa_{1-x}N$ alloys have become very potential for high performance MJ solar cells. Because the band gap of $In_xGa_{1-x}N$ alloys can be varied continuously from 0.7 to 3.4 eV. The $In_xGa_{1-x}N$ films show an exceptionally strong and robust photoluminescence, although it grown on lattice mismatched substrates. It is also shown that the optical and electronic properties of the $In_xGa_{1-x}N$ alloys exhibit a much higher resistance to high-energy (2 MeV) proton irradiation than the currently used photovoltaic materials such as GaAs and GaInP, and therefore offer great potential for radiation-hard high-efficiency solar cell for space applications [1]. The band gap energy of InN has extended the range of the energy gaps of III-nitride alloys from the deep ultraviolet to the practically very important near infrared spectral region. This spectral range provides an almost perfect fit to the full solar spectrum as shown in Fig.1, offering

a unique opportunity to design MJ solar cells using a single ternary alloy system. This will be technologically very significant because of easy fabrication, similarity in thermal expansion coefficient, electron affinity and lattice constant. In addition, InN-based alloys are predicted to show high mobilities and lifetime of charge carriers and superior resistance against irradiation damage. Therefore, $In_xGa_{1-x}N$ alloys are very promising for high performance solar cells. In order to realize the high performance $In_xGa_{1-x}N$-based MJ solar cells theoretical design and performance evaluation are very much essential. Compared to the theoretical work on conventional material based MJ solar cells there is very little work on $In_xGa_{1-x}N$-based MJ solar cells. Bouazzi et al. observed the theoretical possibilities of $In_xGa_{1-x}N$ tandem PV structure [11]. However, the work is very preliminary one and the efficiency was not remarkable. For example, the effect of the depletion region and various parameters on efficiency was not considered. More works on the theoretical design and performance evaluation of $In_xGa_{1-x}N$-based MJ solar cells for high efficiency are urgently required.

In this work, $In_xGa_{1-x}N$-based MJ solar cells have been designed theoretically for high efficiency and the performance of the designed solar cells are evaluated with various parameters. The efficiency has been calculated up to eight junctions. The efficiency can be calculated at any junction number using the developed model. Band gaps are optimized with minimizing the current mismatch for each cell to get the maximum efficiency. The effects of the surface recombination velocity, emitter thickness, doping density and minority carrier life time on efficiency have been studied for $In_xGa_{1-x}N$-based MJ solar cells of both *n* on *p* and *p* on *n* type cells. The efficiency has been also calculated using concentrator system. Unless specified, the evaluated performance shown in this thesis is for $In_xGa_{1-x}N$-based MJ solar cells of *n* on *p* type cells.

1.3 Thesis Organization

In this thesis, the theoretical calculation and optimization of high efficiency $In_xGa_{1-x}N$-based MJ solar cells are performed for high performance photovoltaic systems. The objective of this thesis is to make solar cell competitive with the conventional solar cell to meet the increasing energy demand of the world are discussed in **chapter 1**.

To overcome the difficulties of low conversion efficiency $In_xGa_{1-x}N$ based MJ solar cells have been proposed. The working principle and efficiency losses of solar cell are discussed in **chapter 2**. The approaches to increase the efficiency using MJ technique with considering the fabrication challenges are also discussed.

MJ solar cells are a new technology that offers extremely high efficiencies compared to traditional solar cells made of a single layer of semiconductor material. Decades of research in developing single-material solar cells have led to cell efficiencies close to the theoretical limit. These create the opportunity to design and fabricate $In_xGa_{1-x}N$-based MJ solar cells that will have greatly improved efficiencies, possibly reaching the theoretically predicted ultimate efficiencies. The promising material, $In_xGa_{1-x}N$ and its properties which are used to design the MJ solar cell are discussed in **chapter 3**. Also the cross-sectional view, equivalent circuit, band diagram and theoretical design and modeling of proposed $In_xGa_{1-x}N$-based MJ solar cells are shown.

The design and performance of $In_xGa_{1-x}N$MJ solar cell comprising different number of junction have been investigated theoretically. In **chapter 4,** the performances of $In_xGa_{1-x}N$-based MJ solar cells have been shown. For efficiency maximization the optimized band gap, short-circuit current density, and open-circuit voltage as a function of junction number included in the cell are calculated. The current and lattice mismatch at the interfaces of the different junction have been investigated. The effect of different

parameters such as surface recombination velocity, minority carrier life time, emitter thickness and doping density of carriers on the efficiency have been analyzed for both n-p and p-n MJ solar cells.

In order to compete with greater cost reduction of MJ solar cells, the concentrators are performed for high efficiency photovoltaic systems. The concentrator photovoltaic system and effect of concentrator on efficiency are discussed in **chapter 5**. Also evaluated the effect of temperature under concentrator on efficiency is shown.

Chapter 6 concludes this thesis. This also deals with the summary of this thesis. This also contains the future direction, how to increase the efficiency of solar cell. It proposed the multi sun approach for future work that should be done to achieve better performance of solar cell.

CHAPTER 2
Solar Cell and Efficiency

2.1 Introduction

Solar radiations are a plentiful and clean source of power. Sun emits energies covering a range of wavelengths of the EM spectrum. Photovoltaic is a promising technology that directly takes advantage of our planet's this ultimate source of power. When exposed to light, solar cells are capable of producing electricity without any harmful effect to the environment or device, which means they can generate power for many years while requiring only minimal maintenance and operational costs. The most important drawback of converting solar energy directly to electrical form is low conversion efficiency of commercially available silicon solar cells. Attempts have been made to fabricate photovoltaic cells with materials other than silicon. At the same time modifications in design are being carried out to reduce the reflected component of solar energy. However, still the currently used conventional solar cells show very poor conversion efficiency and poor performance. To overcome these difficulties $In_xGa_{1-x}N$-based multijunction (MJ) solar cells have been proposed. The working principle and efficiency losses of solar cell are discussed in this chapter. The

approaches to increase the efficiency using MJ technique with considering the fabrication challenges are also discussed in this chapter.

2.2 Working Principle of Solar Cell

A simplified schematic diagram of a typical solar cell is shown in Fig. 2.1. Consider a *pn* junction with a very narrow and more heavily doped n-region. The illumination is through the thin n-side. The depletion region *(W)* or the space charge layer (SCL) extends primarily into the *p-side*. There is a built-in field E_0 in this depletion layer. The electrodes attached to the n-side must allow illumination to enter the device. As the n-side is very narrow, most of the photons are absorbed within the depletion region (W) and within the neutral p-side (l_p), and generate electron-hole pairs (EHP) in these regions. Thus the photo-generated EHPs in the depletion region are immediately separated by the built-in field E_0 which drifts them apart. The electron drifts and reaches the neutral n-side whereupon it makes this region negative by an
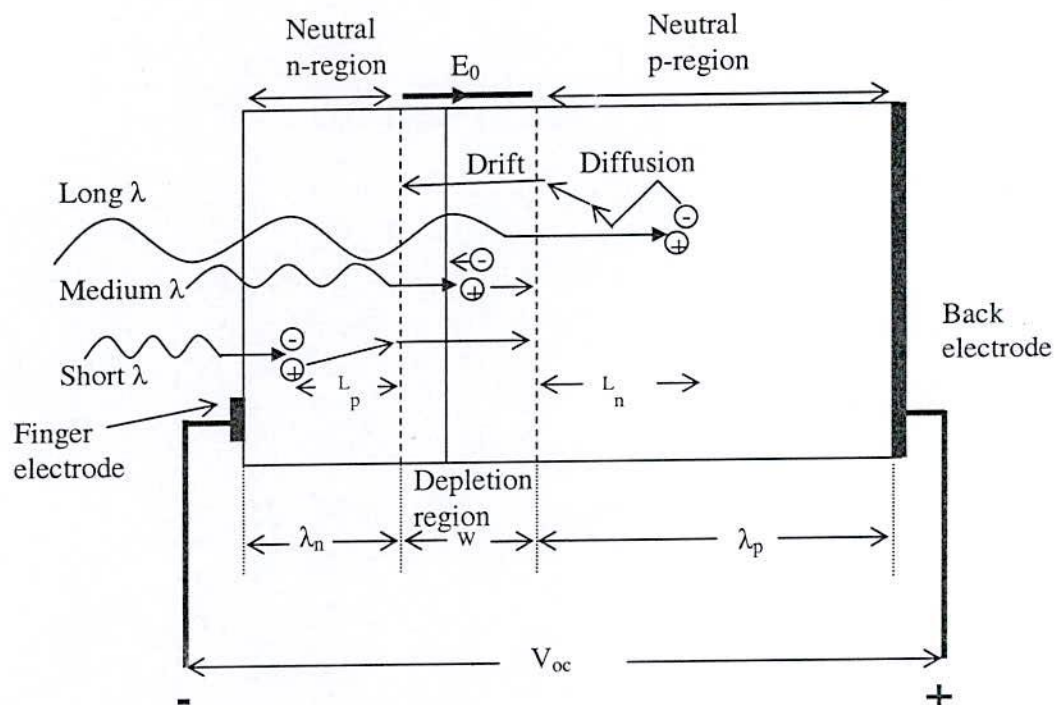
Fig. 2.1 Working principle of Solar cell.

amount of negative charge (–e). Similarly, the hole drifts and reaches the neutral p-side and thereby makes this side positive. Consequently, an open circuit voltage develops between the terminals of the device with the p-side positive with respect to the n-side. If an external load is connected, then the excess electron in the n-side can travel around the external circuit, do work, and reach the p-side to recombine with the excess hole there. It is important to realize that without the internal field E_O it is not possible to drift apart the photogenerated EHPs and accumulate excess electrons on the n-side and excess holes on the p-side.

The EHPs photogenerated by long-wavelength photons that are absorbed in the neutral p-side diffuse around in this region as there is no electric field. If the recombination lifetime of the electron is τ_n, it diffuses a mean distance $L_n = \sqrt{2D_n \tau_n}$ where D_n is its diffusion coefficient in the p-side. Those electrons within a distance L_n to the depletion region can readily diffuse and reach this region whereupon they become drifted by E_o to the n-side as shown in Fig. 2.1. Consequently, only those photogenerated EHPs within the minority carrier diffusion length L_n to the depletion layer can contribute to the photovoltaic effect. Again the importance of the built-in field E_o is apparent. Once an electron diffuses to the depletion region, it is swept over to the n-side by E_o to give an additional negative charge there. Holes left behind in the p-side contribute a net positive charge to this region. Those photogenerated EHPs further away from the depletion region than L_n are lost by recombination. It is therefore important to have the minority carrier diffusion length L_n be as long as possible. The same ideas also apply to EHPs photogenerated by short wavelength photons absorbed in the n-side. Those photogenerated holes within a diffusion length L_p can reach the depletion layer and become swept across to the p-side. The photogeneration of EHPs that contributes to the photovoltaic effect therefore occurs in a region covering $L_p + W + L_n$. If the terminals of the device are shorted as in Fig. 2.2 then the excess electron in the n-side can flow through the external circuit to neutralize the excess hole in the p-side. This current due to the flow of the photogenerated carriers is called the photocurrent.

When the p-type and n-type semiconductors are sandwiched together, the excess electrons in the n-type material flow to the p-type, and the holes thereby vacated during this process. This Process is called diffusion. This diffusion process continues until electric fields develop on either side of junction called depletion region and stops the diffusion of the carrier. This field is called potential barrier, which has the effect of stopping the majority carriers crossing the junction in the opposite direction to the field. However, this field accelerates the minority carriers from both side of the junction, forming the reverse leakage current. A photon incident in or near the depletion region of this cell which has an energy greater than or equal to the band gap of the junction (hv $\geq$ Eg) will excite an electron from the valance band into the conduction band leaving a hole in the valance band. This process is called photogeneration of electron-hole pair (EHP). A carrier pair generated near the junction are separated and swept (drift) across the junction.
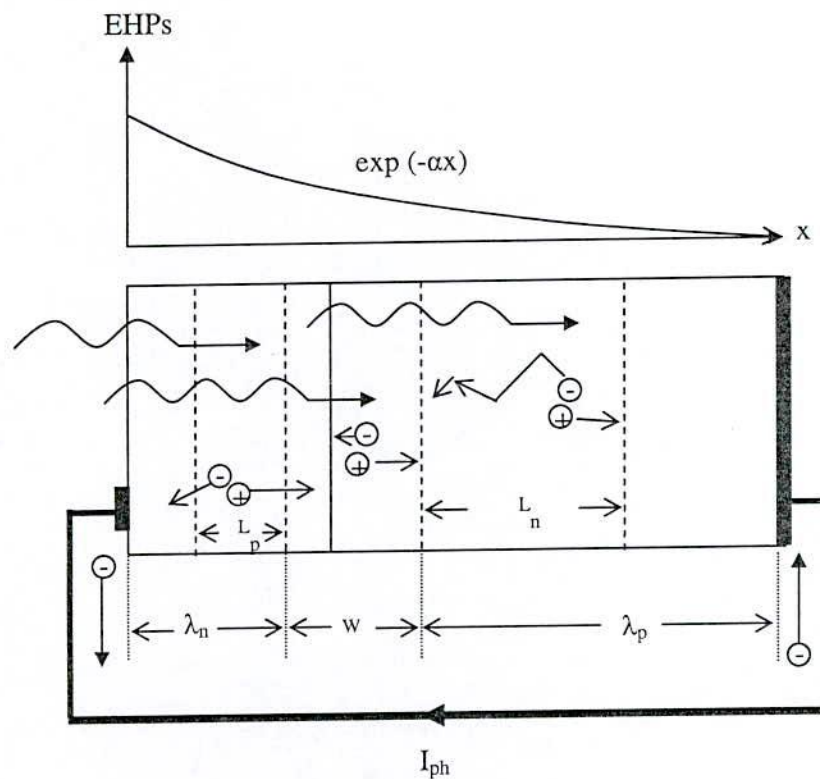
Fig. 2.2 Solar cell operation.

2.3 Efficiency Losses of Solar Cell

Photovoltaic cells are limited in efficiency by many losses, some of these are avoidable but the others are intrinsic to the system. Some limits are obvious and may be controlled independently, but the others are complex and can not be controlled without considering interrelated effects. These are discussed bellow briefly.

2.3.1 Reflection Losses on the Surface

A portion of the incident light that is reflected from the surface of the solar cell is called reflection losses. It has been reduced to almost zero, by means of transparent coatings with appropriate thickness and index of reflection. Losses as low as 3% for silicon cells have been reported in the literature [12]. These losses are no longer major consequence to improve the cell performance.

2.3.2 Incomplete Absorption

Photons with energies equal to or greater than the band gap energy are absorbed in the material as their energy promotes electron into conduction band. If photons have energy exceeding the semiconductor's band gap the excess energy is usually dissipated as heat and thus wasted. In contrast, photons whose energies are less than the band gap energy are transmitted through the material and are not used. The lower the band gap the more photons are absorbed and the greater the number of electron promoted into the conduction band, which generate more current.

2.3.3 Utilization of Only Part of the Photon Energy to Create EHPs.

A large number of the photons that will be absorbed will have more energy than is needed to create an electron-hole pair. Any energy that an impinging photon has in excess of the energy gap of the material will contribute to the lattice vibration of the material and will eventually be dissipated as heat.

2.3.4 Incomplete Collection of EHPs.

A significant number of electron-hole pair generated by photon absorptions will not be created within the space charge region of the n-p junction. Only those pairs created within a diffusion length of the junction can be separated by the built in field. The

majority of those EHPs created at greater distances from the junction will recombine, causing the collection efficiency to fall below 100%.

2.3.5   Voltage Factor V.F.

The largest recoverable voltage in a photo voltaic cell is the open circuit voltage. The open circuit voltage is always observed to be less than the energy gap voltage for the material of which the cell is made. There are two reasons for this: i) The barrier height is equal to the maximum forward voltage across the junction. This is determined by the differences in Fermi levels. Fermi levels are a function of impurity concentration and temperature and are normally located within the forbidden gap thus causing a barrier height to be less than the energy gap. ii) A voltage equal to the barrier height would be obtained only if an extremely large number of electron-hole pairs were generated; this number can never be reached by photon absorption from direct sunlight. $V.F. = V_{OC}/E_g$.

2.3.6   Fill Factor or Curve Factor Loss

The fill factor (FF) is a measure of the junction quality and series resistance of the cell. Figure 2.3 shows the current-voltage (I-V) characteristics of a sample PV cell over its full range of currents and voltages. The characteristic represents the upper
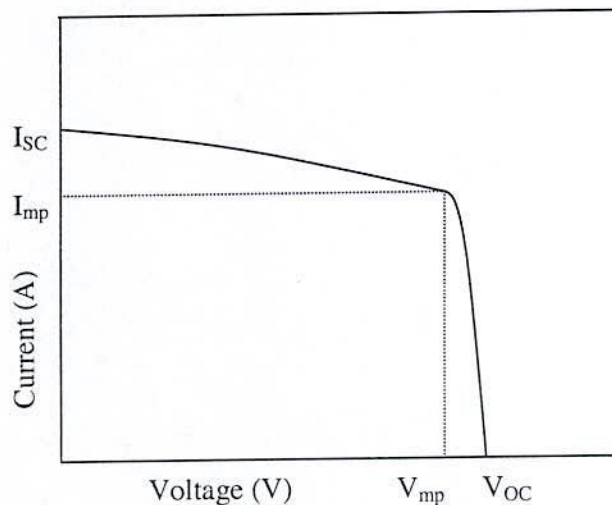
Fig. 2.3 Current- voltage characteristics of a solar cell.

limits for voltage and current of photo voltaic cells. Maximum power voltage, V_{mp} and maximum power current, I_{mp}, are more appropriate measures of actual performance. The performance parameter, fill factor, is commonly used to collectively describe the degree to which V_{mp} matches V_{OC} and I_{mp} matches I_{SC}. Fill factor is given by the following relation.

Fill factor, $FF = (I_{mp} \times V_{mp})/(V_{OC} \times I_{SC})$,

and the maximum power, $P_{max} = I_{mp} \times V_{mp}$

Thus, $FF = P_{max}/(V_{OC} \times I_{SC})$

Fill factors for high efficiency cells are typically in the range of 80% to 90%, where 100% would be ideal.

2.3.7 Recombination Before Drift

Another important loss is the recombination of photo excited electron hole pair before drifting by the depletion layer to create photocurrent. This is happened due to short diffusion length compared to the thickness of the cell structure or due to short life time of the carrier. This loss can be kept to a minimum by using semiconductor with appropriate properties especially long life time for the photogenerated carrier. This can also be done by eliminating all unnecessary defects.

2.3.8 Series and Shunt Resistance

The series resistance of the cell can cause deviation from the ideal voltage-current characteristics. This deviation causes the curve to flatten, resulting in a reduction in the net power output. If the layer of material on the top of the junction reduces in thickness, the collection efficiency improves because of the larger photon absorption. This solution, however, conflicts with resistance requirements, because as the layer is reduced in thickness, its resistance goes up. The ohmic contacts applied to the cell also cause its resistance to increase, but improvement in the techniques of applying contacts have caused this resistance to become negligible. Loss due to shunt resistance is negligible (0.1%) and due to series resistance is 0.3%.

2.3.9 Top Surface Contact Obstruction

The electric current leaves the top surface by a web of metal contact arranged to reduce series resistance, losses in the surface. These contacts on the top of the surface have a finite area and so they cover the active surface which results the reduction of the active surface to absorb light. This loss is not always counted for efficiency calculation.

2.4 Approaches to Increase Efficiency of solar Cells

The goal for photo voltaic energy conversion is the development of high efficiency, low cost photo voltaic structures which can reach the thermodynamic limit of solar energy conversion. Recently, many approaches have been suggested on how to reach these efficiency limits. Recent studies demonstrate that there are a large range of approaches that may be used to reach the efficiency limit of solar energy conversion [13-15]. These are discussed below.

2.4.1 Multiple Junction Solar Cells

Multiple junction solar cells, or tandem solar cells, consist of a multiple, single junction solar cells stacked on one another, with each solar cell absorbing part of the solar spectrum closest to its band gap. Existing tandem devices have achieved efficiencies over 37% [16], and further efficiency increases can be achieved by increasing the number of junctions. Despite the high efficiency potential, tandem devices have an inherent drawback: the efficiency of a tandem is tied to the material quality and the existence of materials with a specified band gap, often using less common or understood material systems. Consequently, the key promise of the new approaches to solar cells that achieve their thermodynamic limit involves decoupling the need for a large number of ideal materials from solar cell efficiency.

2.4.2 Multiple Spectrum Solar Cells

Multiple spectrum solar cells involve the transformation of the solar spectrum from one with a broad range of energies to one with the same power density but a narrow range of photon energies. The central feature of these approaches, which include up and down-conversion [17] and thermo photonics, is that the transformation of the

solar spectrum is done separately from the solar cell itself, thus increasing the efficiency of an existing solar cell structure via additional coatings. This technology could be applied to any solar cell provided that power gained through spectral alternation offsets the cost of the additional optical coating. As many of the suggested approaches can potentially be implemented in a low cost fashion, multiple spectrum solar cells primarily offer a mechanism for relatively moderate efficiency increases using existing solar cell technology.

2.4.3 Multiple Absorption Path Solar Cells

A central limitation of existing solar cell approaches is the one-to-one relationship between an absorbed photon and a generated electron-hole pair. This relation can be circumvented via either two photon absorption (TPA), in which two photons are absorbed to generate a single electron-hole pair, or via impact ionization (also called Auger generation), in which a single high energy photon generates multiple electron-hole pairs. Although such absorption processes have been measured in bulk materials [18], nano-structured materials are required in order to measure a large effect. For example, nano-structured materials have demonstrated high two-photon absorption and impact ionization processes, with close to 100% impact ionization reported [19].
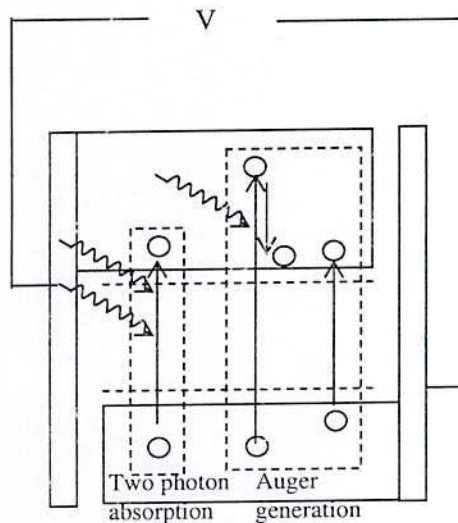
Fig. 2.4 Absorption in multiple absorption path solar cells.

While high impact ionization or TPA rates are an important first step, such high rates alone do not insure high solar cell efficiency, and the critical measurement for such devices is to demonstrate quantum efficiencies substantially exceeding unity.

2.4.4 Multiple Energy Level Solar Cells

In multiple energy level solar cells, the mismatch between the incident energy of the solar spectrum and a single band gap is accommodated by introducing additional energy levels such that photons of different energies can be efficiently absorbed. Multiple energy level solar cells can be implemented either as localized energy levels (first suggested as a quantum well solar cell) or as continuous mini-bands (also called intermediate band for the first solar cell to suggest this approach). Both cases, which are shown in Fig. 2.5, have a fundamental similarity in that the key issue is the generation of multiple light-generated quasi-Fermi levels. The transport of the carriers between the two approaches, however, is substantially different. In the mini-band case, the transport must occur along the mini-bands and hence the carriers must not be able to thermalize from one band to another. This means that the density of states must be zero between the bands, and hence that such approaches must use either quantum dots or a material which inherently has multiple bands. In localized energy
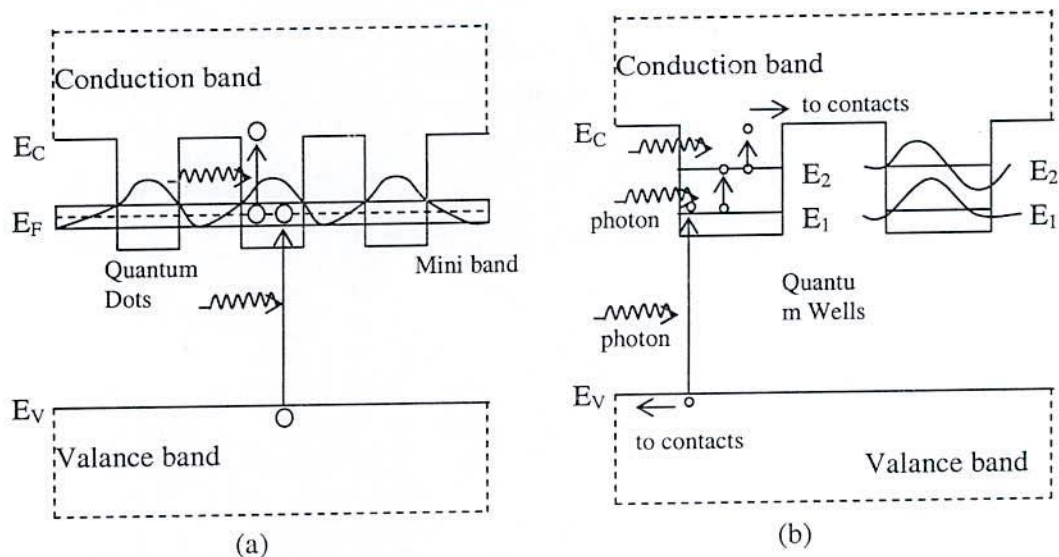
Fig. 2.5 Implementation of multiple energy level solar cells.

level approaches, transport is accomplished by having the carriers at each localized energy level escape by light absorption. To maintain high collection efficiency, the escape time should be faster than the recombination time. The feasibility of the escape process is well demonstrated by quantum-well infrared photodetectors, which have high collection from intra-sub band processes. Localized band approaches have a further advantage in that successive localized energy levels can have different energies, thus allowing a large number of effective band gaps and high efficiencies.

2.4.5 Multiple Temperature Solar Cells

A solar cell which contains multiple temperatures in a single device can use these temperature differentials to generate power. The multiple temperatures may be due to variations in the physical temperature of the lattice, but it is easier to maintain a temperature differential between hot carriers and thermalized carriers. The multiple temperature approach has the advantage that a thermal converter allows higher efficiencies given identical high concentration structures. A thermal converter can be implemented by a structure in which the band edges in the converter vary, allowing interactions between hot carriers and carriers at the band edge. While this approach allows efficiencies 66% with three energy levels, the physical effect of thermal interactions have not been demonstrated.

2.5 Multijunction: An Exciting Approach to High Efficiency

Efficiency can be increased by reducing loss due to band gap mismatch (which is the major cause of low efficiency) by using MJ solar cells. It can make better use of the solar spectrum by having multiple semiconductor layers with different band gaps. Each layer is made of a different material, which usually is an III-V semiconductor, and absorbs a different portion of the spectrum. The top layer has the largest band gap so that only the most energetic photons are absorbed in this layer. Less energetic photons must pass through the top layer since they are not energetic enough to generate EHPs in the material. Each layer going from the top to the bottom has a smaller band gap than the previous. Therefore, each layer absorbs the photons that
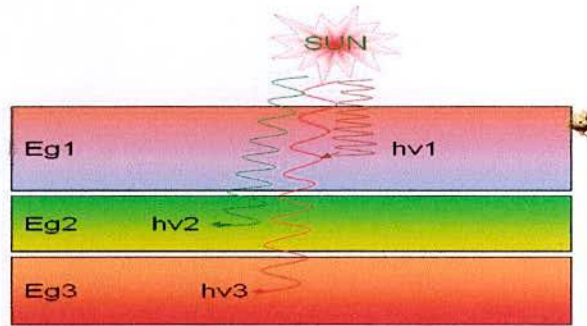
Fig. 2.6 A simple presentation of MJ solar cells.

have energies greater than or equal to the band gap of that layer and less than the band gap of the higher layer. In this way there arises a perfect utilization of the full solar spectrum and increased efficiency. Existing tandem devices have achieved efficiencies over 37% for a triple junction cell. Theoretically the efficiency of MJ solar cells increase as it incorporates more and more junctions.

2.6   Major Fabrication Challenges of Monolithic MJ Solar Cells

A monolithic MJ solar cells experiences four major fabrication challenges. These are band gap, lattice matching, current matching and tunnel junctions, which are discussed in the following section. Band gap and lattice matching are central to MJ solar cells designs.

2.6.1   Band gap Matching

Since the band gaps of the materials used in a MJ solar cells determine which layer a photon is absorbed in, the band gaps determine how much energy can be obtained from each photon. Ideally the difference between adjacent layers of the solar cell is approximately constant so that each layer can absorb an equal amount of the spectrum of incident light. Since the amount of excess energy from light converted to heat is equal to the difference between the photon energy and the band gap of the absorbing material, the difference between band gaps should be made as small as possible. Also the solar cell should take advantage of as much of the spectrum as possible so the top layer should have a high band gap and the bottom layer should have a small band gap.

There is a design tradeoff for a given number of layers of a MJ solar cells between having the band gaps differ by a small amount and have the band gaps cover a large range of the spectrum.

2.6.2 Lattice Matching

In monolithic MJ solar cells, the different semiconductor layers are grown directly on top of the other layers using the same substrate. As a result of this method, the lattice constant, which describes the spacing between the atoms of a crystal structure, should be the same for all of the layers. Research at the National Renewable Energy Laboratory (NREL) showed that a lattice mismatch as small as 0.01% significantly decreases the current produced by the solar cell. The restriction of each semiconductor material having the same lattice constant significantly decreases the
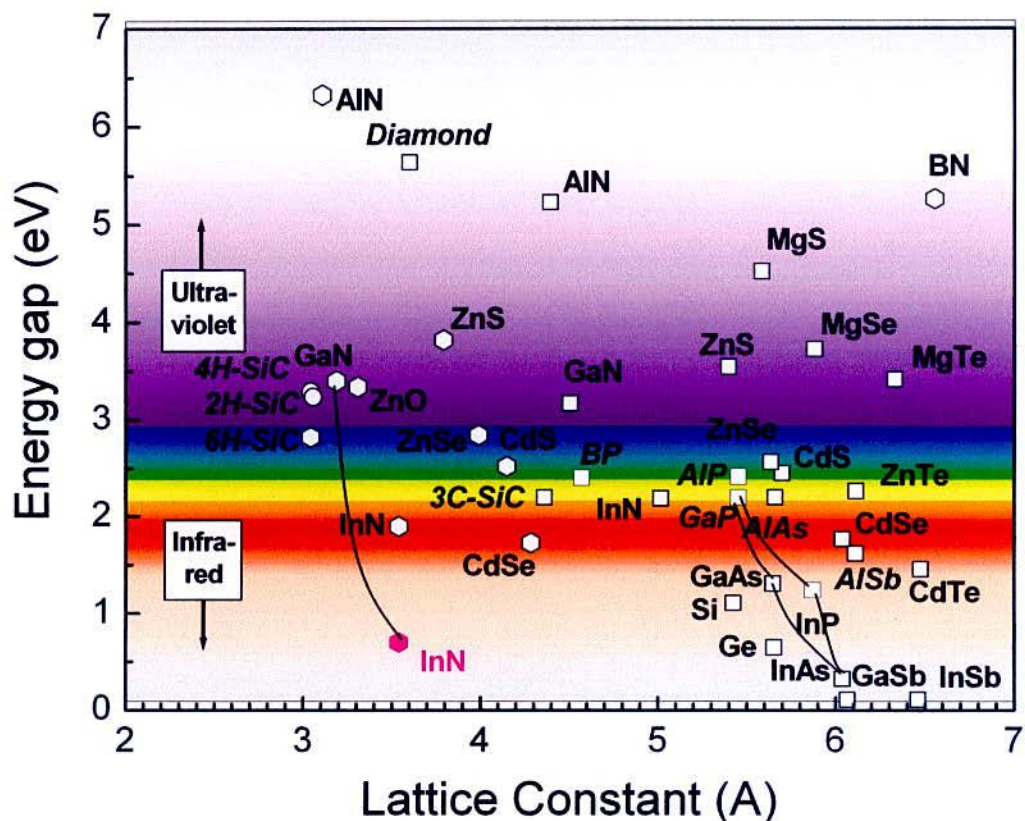
Fig. 2.7 Relationship between band gap energies and lattice constants of the semiconductors important for optoelectronics [20].

number of materials that may be used. Figure 2.7 shows the lattice constant and band gap of common semiconductor materials. Lines between different materials represent semiconductors that are created by combining different amounts of the two materials. The vertical line passing through from InN to GaN represents the materials that are proposed to design MJ cells made of $In_xGa_{1-x}N$ with different composition of In. One should choose materials that have the same lattice constant, but different band gaps. Hence, monolithically stacking the two material results in a lattice matched compound with different band gaps, minimizing the thermal losses and maximizing the efficiency.

2.6.3 Current Matching

Since the current flows through a solar cell from the top to the bottom, the layers of a MJ solar cells are in series. Therefore, the current passing through each layer must be the same and the current produced by the solar cell is limited by the layer that produces the least amount of current. For maximum efficiency, the cell must be designed so that each layer produces the exact same current. The current is proportional to the number of photons absorbed in each layer. The two most important factors in determining the thickness of each layer is the number of photons in the spectrum that the layer should absorb and the absorption constant of the material. The light intensity decreases exponentially with penetration depth into a material where the exponential constant is called the absorption constant. A layer with a low absorption constant must be made thicker since on average a photon must pass through more of the material before it is absorbed. Properly designing the thickness of each semiconductor material based on these factors will match the current produced by each layer.

2.6.4 Tunnel Junction

Tunnel junctions are placed between the layers of a MJ to avoid the formation of junction as well as potential barrier between the layers. The tunnel junction is fabricated by doping the semiconductor material that will form the P-N junction at a level one hundred to several thousand times that of a typical semiconductor diode. This will result in greatly reduced depletion region, of the order of magnitude of 10⁻

^{6}cm, or typically about 1/100 the width of this region for a typical semiconductor diode. It is this thin depletion region that many carriers can 'tunnel' through, rather than attempt to surmount, at low forward bias potentials that account for the peak in the curve (Fig 2.8). For comparison, a typical semiconductor diode characteristic has been superimposed on the tunnel diode characteristics. This reduced depletion region
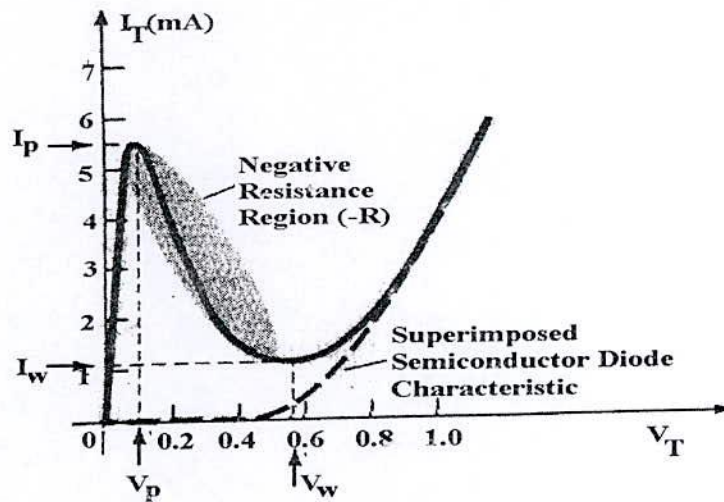
Fig. 2.8 Characteristics of tunnel junction.
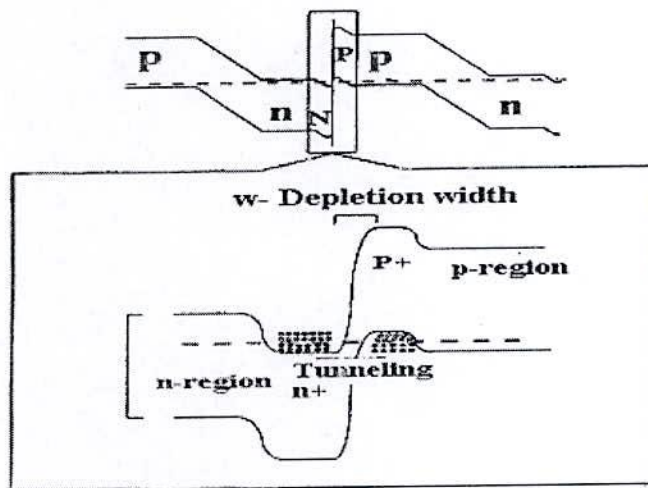
Fig. 2.9 Tunneling of MJ solar cell.

results in carriers 'punching through' at velocities that far exceed those available with the conventional diode. The doping scheme used in MJ solar cells to promote tunneling at junction as shown in Fig 2.9. When the photogenerated electron from p region being swept across the junction to the n region, the Fermi level in the n+ region would rise with respect to the p+ region, aligning electron with empty states. These electrons would then tunnel through the thin junction, allowing current to flow through the cell. One problem encountered when creating a tunnel junction is that when the cell is annealed at high temperature, the tunnel junction may diffuse out of the junction, widening the depletion region. The wide depletion region reduces tunneling and limits the current that can be carried in the cell.

CHAPTER 3
Design of InGaN-based MJ Solar Cells

3.1 Introduction

Multijunction (MJ) solar cell technology offers high efficiencies compared to traditional solar cells made of a single layer of semiconductor material. Currently used MJ solar cells are based on two or three junctions of different materials which are usually III-V semiconductors, and absorb a different portion of the solar spectrum. Recently $In_xGa_{1-x}N$ alloys have become very promising materials for high performance MJ solar cells. This creates an opportunity to design and fabricate $In_xGa_{1-x}N$-based MJ solar cells that will have greatly improved performance. In order to realize such solar cell proper theoretical design for high performance is urgently required. Therefore, the theoretical design and modelling for high efficiency $In_xGa_{1-x}N$-based solar cells are discussed in this chapter. The properties of the promising material, $In_xGa_{1-x}N$, which are used to design the MJ solar cells, are also discussed in this chapter. Also the cross-sectional view, equivalent circuit and band diagram of the proposed $In_xGa_{1-x}N$-based solar cells are shown.

3.2 Properties of In$_x$Ga$_{1-x}$N

Some properties of the identified In$_x$Ga$_{1-x}$N alloys are not available in literature. In such cases data of GaN is considered. The majority carrier concentration was taken equal to 10^{18} cm^{-3} on each side of the junction. The electronic properties of the identified In$_x$Ga$_{1-x}$N alloys are assumed to be same in all junctions and are supposed to be equal to those of the GaN, which are taken from references [21, 22]. The surface and the rear recombination velocities were taken to be equal to 10^3 cm/s.

L_n= 125 × 10^{-6} cm, L_p= 79 × 10^{-6} cm,

D_p = 9 cm^2/s, D_n = 25 cm^2/s.

More accurate material parameters may improve the efficiency, since diffusion length and diffusion coefficient of InN-based alloys are expected to be higher than GaN. Others parameters of In$_x$Ga$_{1-x}$N are described below.

3.2.1 Band gap Energy

Approximate calculations were performed in order to identify the band gaps energy, E_g, of the In$_x$Ga$_{1-x}$N alloys that are used for the tandem cell. These approximate calculations were done assuming a perfect quantum response of the materials and
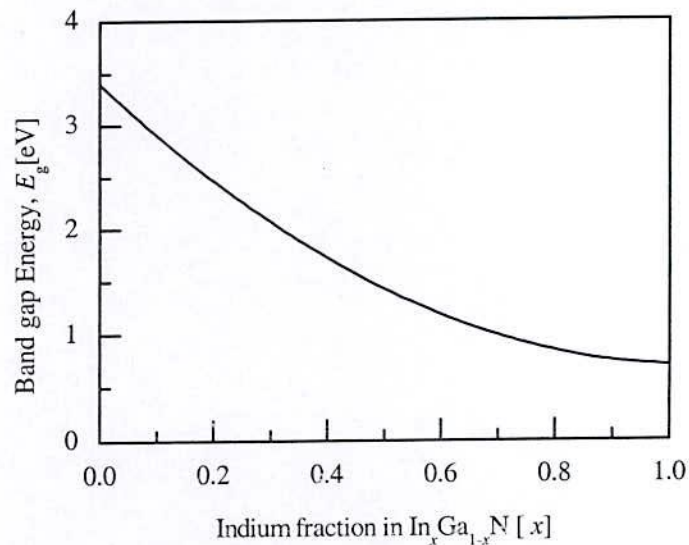
Fig. 3.1 Calculated band gap from the Eq. 3.1.

equal photocurrent densities for all of the junctions of the tandem cell. The indium fraction, x was calculated by the following equation [23]

$$E_{g_{InGaN}}(x) = (1-x)E_{g_{GaN}} + xE_{g_{InN}} - bx(1-x) \qquad (3.1)$$

where, energy gaps $E_{g_{GaN}}$ and $E_{g_{InN}}$ are equal to 3.4 and 0.7 eV, respectively and bowing parameter $b = 2.5$eV ($In_xGa_{1-x}N$). The compositional dependence of the band gap energy in $In_xGa_{1-x}N$ material is shown Fig. 3.1.

3.2.2 Absorption Coefficient, α

When light impinges on a semiconductor with photon energy, hv, greater than or equal to the band gap energy, E_g, which is absorbed, results in the excitation of an electron from the valence band to the conduction band. The absorption coefficient, α, is a material parameter which depends on the photon energy. It is a measure of how good the material is for absorbing light of certain wave length. Absorption coefficient in $In_xGa_{1-x}N$ is related to its composition i.e. In fraction, x as well as wave length of the light. It also depends on temperature of operation. The absorption coefficient of $In_xGa_{1-x}N$ alloys as a function of photon energy with different indium composition is shown in Fig. 3.2 at room temperature (300° K).
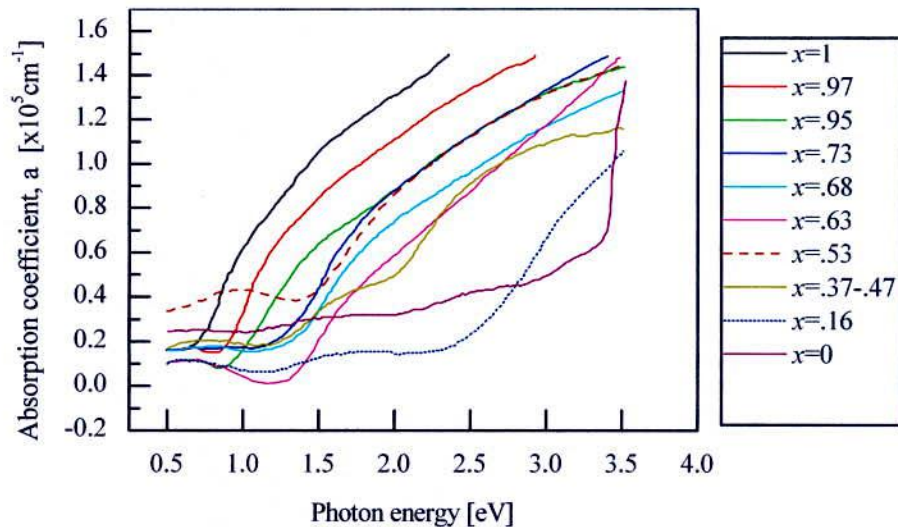
Fig. 3.2 Absorption coefficient of $In_xGa_{1-x}N$ alloys as a function of photon energy with different indium composition, x [24].

3.3 InGaN-based Multijunction Solar Cell

3.3.1 Cross-Sectional View
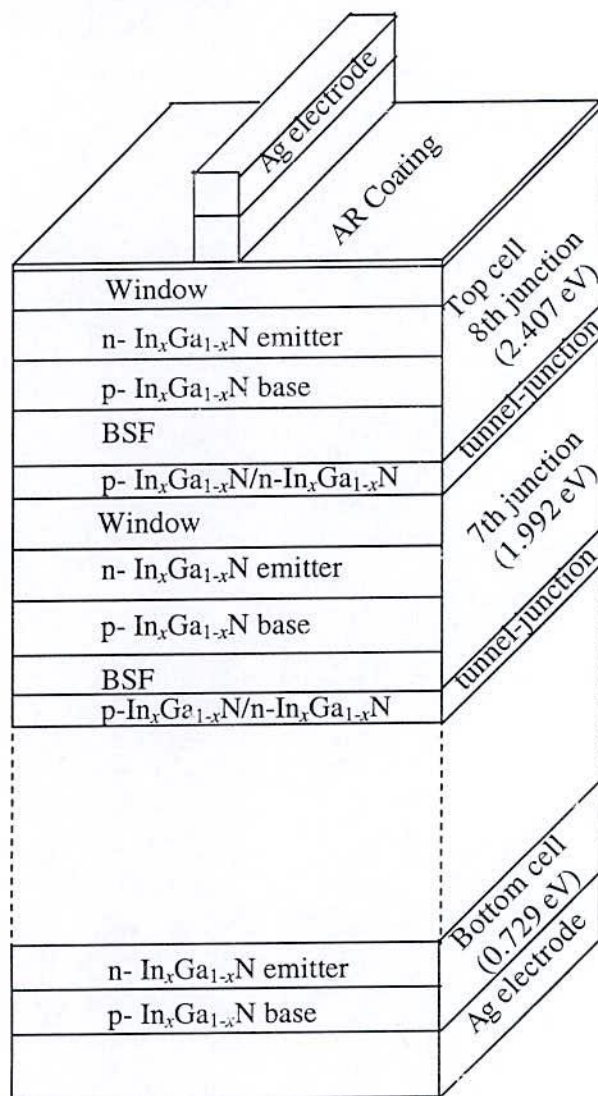
Fig. 3.3 Schematic illustration of the proposed $In_xGa_{1-x}N$ solar cells for 8 junctions.

Figure 3.3 shows a schematic illustration of the proposed $In_xGa_{1-x}N$ MJ solar cells. All the subcells are made of $In_xGa_{1-x}N$ alloy with different composition to obtain the required band gap. The subcells are arranged from bottom to top with lower to higher the band gap. Tunnel junctions are placed between the layers of a MJ to avoid the formation of junction as well as potential barrier between the layers.

3.3.2 Band Diagram
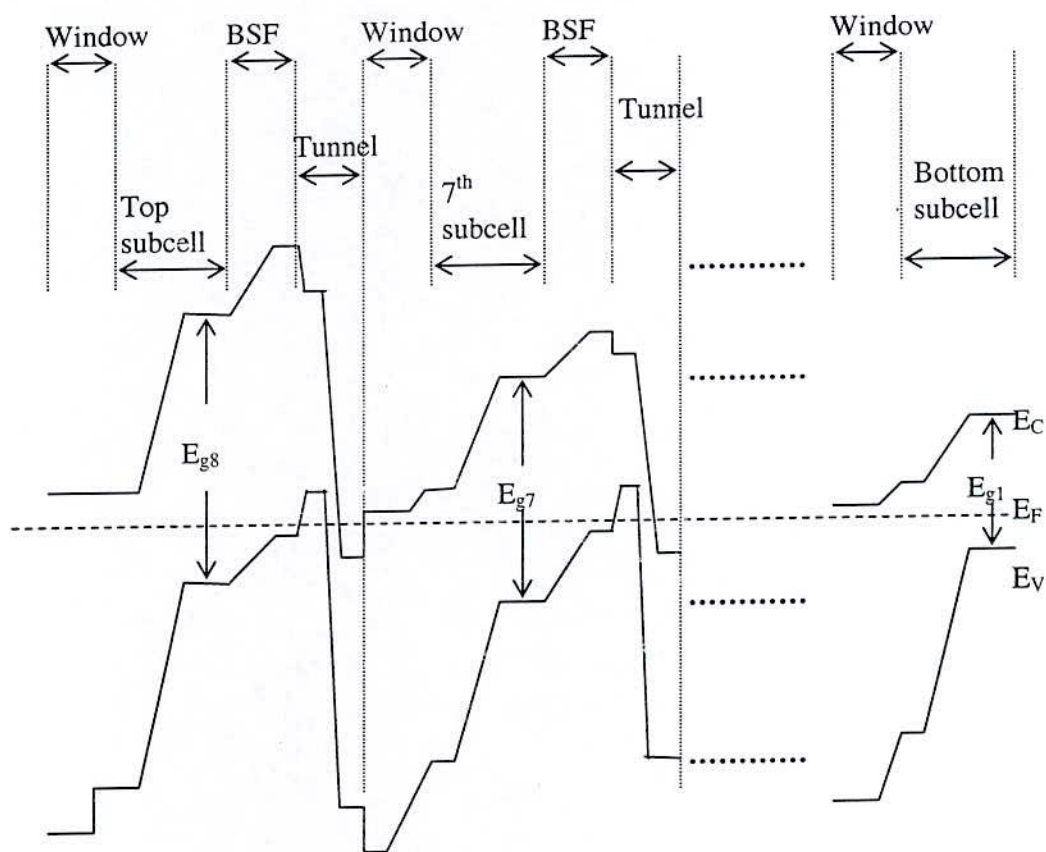
Fig. 3.4 Band diagram of the proposed In$_x$Ga$_{1-x}$N solar cells.

The band diagram of the proposed In$_x$Ga$_{1-x}$N solar cells is shown in Fig. 3.4. The band gap energies of the window layer and back surface field (BSF) layer are higher than that of respective junction which reflect holes and electrons, and reduce the carrier recombination. Also, a high-band gap window layer reduces the cell's series resistance.

3.3.3 Equivalent Circuit

(a) Single- unit model (b) Multi- unit model
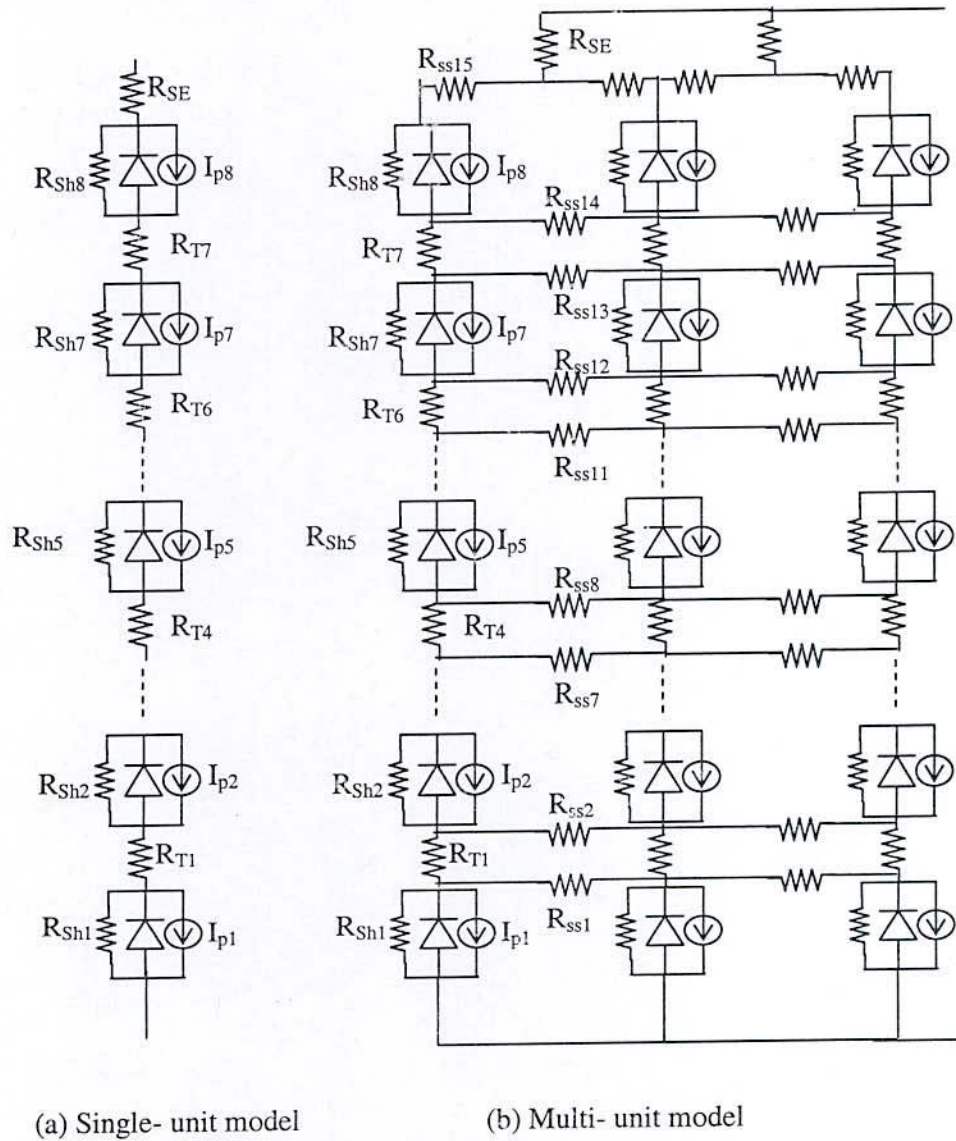
Fig. 3.5 Equivalent circuit of proposed $In_xGa_{1-x}N$-based solar cell.

Figure 3.5 shows the circuit models of the proposed $In_xGa_{1-x}N$-based eight-junction solar cells using the single-unit model and multi-unit model. As shown in Fig. 3.5 (a), the single-unit model is composed of eight diodes connected in series. In the multi-unit model, as shown in Fig.3.5 (b), the same numbers of units are installed and the units are connected to each other via lateral resistances (R_{ss1} to R_{ss15}) for practically fabricated MJ solar cells. The series resistance of solar cells consists of various

components such as resistance due to electrodes (R_{SE}), lateral resistance between each electrode (R_{SL}) and tunnel junctions (R_T).

3.4 Theoretical Design and Modeling

Efficiency evaluation includes calculation of the total number of photons in solar spectrum per unit area per unit time and selection of band gap in each junction so that equal number of photon can be absorbed. The photocurrent density is calculated in each junction due to absorption of photons to determine the short circuit current density (J_{SC}). The current mismatch between the junctions in the cells has been minimized by adjusting the emitter thickness. To obtain the maximum efficiency, the bottom junction band gap energy is optimized and then the other junction's band gap energies are selected accordingly. Also open circuit voltage V_{OC} is calculated.

3.4.1 Photocurrent Density

When a monochromatic light of wavelength λ is incident on the front surface, the photocurrent and spectral response, that is the number of carriers collected per incident photon at each wavelength, can be derived as follows. The generation rate of EHPs at a distance x' from the semiconductor surface is given by [35]

$$G(\lambda, x') = \alpha(\lambda)F(\lambda)[1 - R(\lambda)]e^{[-\alpha(\lambda)x']} \tag{3.2}$$

where, $\alpha(\lambda)$ is the absorption coefficient, $F(\lambda)$ the number of incident photons/cm^2/s per unit bandwidth and $R(\lambda)$ is the fraction of these photons reflected from the surface. Under low injection condition, the one dimensional steady-state continuity equations for electrons in p-type and holes in n-type semiconductors are

$$G_n - \frac{n_p - n_{po}}{\tau_n} + \frac{1}{q}\frac{dJ_n}{dx'} = 0 \tag{3.3}$$

and

$$G_p - \frac{p_n - p_{no}}{\tau_p} + \frac{1}{q}\frac{dJ_p}{dx'} = 0 \tag{3.4}$$

respectively. The current density equations for electron and hole are

$$J_n = q\mu_n n_p \xi + qD_n \frac{dn_p}{dx'} \tag{3.5}$$

and

$$J_p = q\mu_p p_n \xi - qD_p \frac{dp_n}{dx'} \qquad (3.6)$$

respectively.
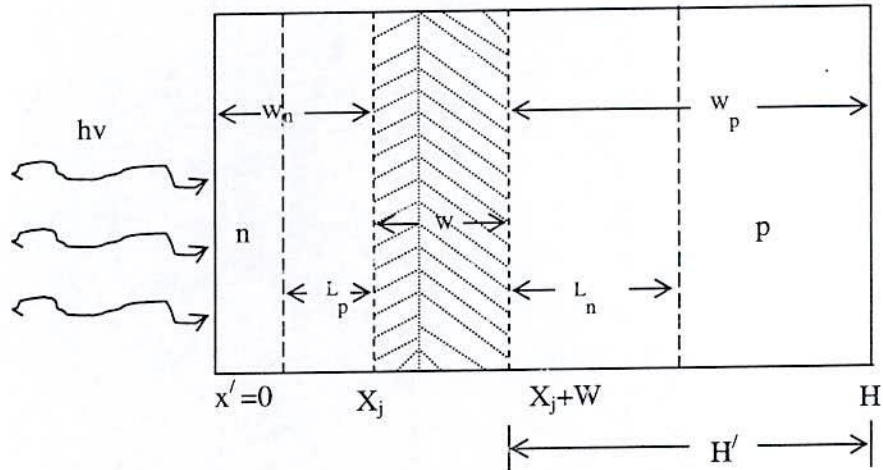
Fig. 3.6 Solar cell dimensions and minority-carrier diffusion lengths.

Here,

L_p= Diffusion length for p-type

L_n = Diffusion length for n-type

S_p = Recombination velocities in p-type

S_n = Recombination velocities in n-type

D_p = Diffusion coefficient for p-type

D_n = Diffusion coefficient for n-type

X_j= Thickness of n-type material

H'= Thickness of p-type material

W= Depletion width

H= Width of the entire cell.

For an abrupt *n-p* junction solar cell with constant doping on each side of the junction, there are no electric fields outside the depletion region of Fig. 3.6. In the case of an *n* on *p* junction with an n-type emitter and p-type base Eqs. (3.2), (3.4) and (3.6) can be combined to yield an expression for the top side of the junction.

$$D_p \frac{d^2 p_n}{dx'^2} + \alpha F (1-R) e^{(-\alpha x')} - \frac{p_n - p_{no}}{\tau_p} = 0 \tag{3.7}$$

The general solution of this equation is

$$p_n - p_{no} = A \cosh(x'/L_p) + B \sinh(x'/L_p) - \frac{\alpha F(1-R)\tau_p}{\alpha^2 L_p^2 - 1} e^{(-\alpha x')} \tag{3.8}$$

where, $L_p = \sqrt{(D_p \tau_p)}$ is the diffusion length. There are two boundary conditions. At the surface, $x' = 0$, we have surface recombination with a recombination velocity S_p:

$$D_p \frac{d(p_n - p_{no})}{dx} = S_p (p_n - p_{no}) \tag{3.9}$$

At the edge of the depletion region, $x' = x_j$ the excess carrier density is small due to the electric field in the depletion region:

$$p_n - p_{no} \cong 0 \tag{3.10}$$

Substituting Eq. (3.9) and (3.10) into Eq. (3.8), the hole density is

$$p_n - p_{no} = [\alpha F (1-R)\tau_p / (\alpha^2 L_p^2 - 1)] \times$$

$$\left[\frac{(\frac{S_p L_p}{D_p} + \alpha L_p) \sinh(\frac{x_j - x'}{L_p}) + e^{-\alpha x_j} (\frac{S_p L_p}{D_p} \sinh\frac{x'}{L_p} + \cosh\frac{x'}{L_p})}{\frac{S_p L_p}{D_p} \sinh(x_j / L_p) + \cosh(x_j / L_p)} - e^{-\alpha x'} \right] \tag{3.11}$$

and the resultant hole photocurrent density at the depletion edge is J_p.

$$J_p = [qF(1-R)\alpha L_p / (\alpha^2 L_p^2 - 1)] \times$$

$$\left[\frac{(\frac{S_p L_p}{D_p} + \alpha L_p) - e^{-\alpha x_j} (\frac{S_p L_p}{D_p} \cosh(x_j / L_p) + \sinh(x_j / L_p))}{\frac{S_p L_p}{D_p} \sinh(x_j / L_p) + \cosh(x_j / L_p)} - \alpha L_p e^{-\alpha x_j} \right] \tag{3.12}$$

This photocurrent would be collected from the front side of an n on p junction solar cell at a given wavelength assuming this region to be uniformed in lifetime, mobility,

and doping level. To find the electron photocurrent collected from the base of the cell Eqs. (3.2), (3.3), (3.5) are used with the following boundary conditions,

$$\text{at } x' = x_j + W , \; n_p - n_{po} \cong 0 \tag{3.13}$$

and at $x' = H'$, $S_n(n_p - n_{po}) = -D_n dn_p / dx'$ (3.14)

Using the boundary conditions the electron density is

$$n_p - n_{po} = \frac{\alpha F (1-R)\tau_n)}{(\alpha^2 L_n^2 - 1)} e^{[-\alpha(x_j+W)]} \{ \cosh(\frac{x'-x_j-W}{L_n}) - e^{-[\alpha(x'-x_j-W)]} -$$

$$\frac{(\frac{S_n L_n}{D_n})[\cosh(\frac{H'}{L_n}) - e^{(-\alpha H')}] + \sinh(H'/L_n) + \alpha L_n e^{-\alpha H'}}{\frac{S_n L_n}{D_n} \sinh(H'/L_n) + \cosh(H'/L_n)} \times \sinh(\frac{x'-x_j-W}{L_n}) \} \tag{3.15}$$

and the photocurrent density due to electrons collected at the depletion edge is J_n.

$$J_n = [qF (1-R)\alpha L_n / (\alpha^2 L_n^2 - 1)] e^{-\alpha(x_j+W)}$$

$$\times \left[\alpha L_n - \frac{(\frac{S_n L_n}{D_n})[\cosh(H'/L_n) - e^{-\alpha H'}] + \sinh(H'/L_n) + \alpha L_n e^{-\alpha H'})}{\frac{S_n L_n}{D_n} \sinh(H'/L_n) + \cosh(H'/L_n)} \right] \tag{3.16}$$

Some photocurrent generation takes place within the depletion region. The photocurrent per unit bandwidth is equal to the number of photons absorbed.

$$J_{dr} = qF(1-R)e^{(-\alpha x_j)}[1 - e^{(-\alpha W)}] \tag{3.17}$$

Total photocurrent at a given wavelength:

$$J(\lambda) = J_p(\lambda) + J_n(\lambda) + J_{dr}(\lambda) \tag{3.18}$$

The spectral response is equal to $SR(\lambda) = \dfrac{J(\lambda)}{qF(\lambda)[1-R(\lambda)]}$ (3.19)

The total photocurrent density obtained from the solar spectral distribution F (λ) is given by [35]

$$J_{ph} = q \int_0^{\lambda_m} F(\lambda)[1 - R(\lambda)SR(\lambda)d\lambda \qquad (3.20)$$

where, λ_m is the longest wavelength corresponding to the semiconductor band gap.

In a MJ solar cells, the top junction with higher energy gap absorbs the photons with energy greater or equal to its energy gap E_{g1}, which produce a photocurrent density J_{ph1} and transmit the remaining photons to the junction directly below, and so on until the bottom junction of the tandem cell. The short circuit current density of a tandem cell J_{SC} is given by the least of the photocurrent densities produced by the junctions of the tandem solar cell. J_{SC} equal to Minimum (J_{phi}), where, $i=1,2,3...n$, and n is the number of junction incorporated in the tandem solar cell and J_{phi} is photo current density of ith junction. The photocurrent density J_{ph} of an n-p junction with energy gap $E_g(i)$ and receiving light from n-side is given by [11]

$$J_{Phi} = \sum_{AM\ 1.5} J_{Pi}(\lambda) + J_{ni}(\lambda) + J_{dr}(\lambda), \ E_g(i) \leq hv \qquad (3.21)$$

where, $J_{pi}(\lambda)$, $J_{ni}(\lambda)$ and $J_{dr}(\lambda)$ are respectively the holes, electrons and depletion region current densities produced by the photons of energy $hv \geq E_g(i)$.

3.4.2 Open Circuit Voltage

Form the equivalent circuit of solar cell shown in Fig. 3.7.

$$J = J_d - J_{ph} \qquad (3.22)$$

Therefore, the Eq. (3.22) can be written as

$$J = J_0(e^{qv/kT} - 1) - J_{ph} \qquad (3.23)$$

$$\text{where, } J_d = J_0(e^{qv/kT} - 1)$$

The open circuit voltage can be obtained from Eq. (3.23) with $J=0$

Therefore, the open circuit voltage for an n-p junction is given by

$$V_{oc} = \frac{kT}{q} \times \ln\left(\frac{J_{ph}}{J_0} + 1\right) \qquad (3.24)$$
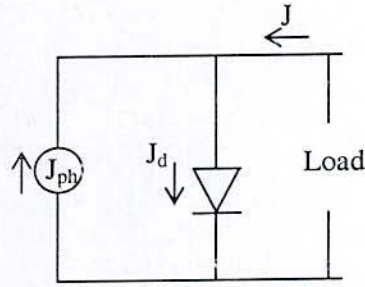
Fig. 3.7 Ideal equivalent circuit of solar cell.

where, J_{ph} is the junction photo current density,

J_0 is the saturation current density,

k is the Boltzmann constant,

T is the temperature which was taken equal to 300°K,

q is elementary electron charge density.

The saturation current density J_0 was calculated for all the $In_xGa_{1-x}N$ alloys using the following relationship [11].

$$J_0 = qn_i^2 \left(\frac{D_{nj}}{L_{nj} N_A} + \frac{D_{pj}}{L_{pj} N_D} \right) , \quad j=1, 2 \dots n \tag{3.25}$$

where, N_A is the concentration of accepter atoms per cm^3 on the p side, N_D is concentration of donor atoms per cm^3 on the n side, n_i is the intrinsic carrier concentration, j is the number of jth junction.

The intrinsic carrier concentration is given by the following equation.

$$n_i^2 = N_C N_V \exp\left(-\frac{E_g}{kT} \right) \tag{3.26}$$

where, N_C =density of states for conduction band, and N_V = density of states for valence band.

$$N_c = 4.3 \times 10^{14} \times T^{3/2} \ (cm^{-3}) \tag{3.27}$$

$$N_v = 8.9 \times 10^{15} \times T^{3/2} \ (cm^{-3}) \tag{3.28}$$

The values of N_C and N_V can be given by [25].

Using Eqs. (3.27) and (3.28), (3.28) can be expressed by

$$n_i^2 = 3.827 \times 10^{29} \times T^3 \exp\left(-\frac{E_g}{kT}\right) \tag{3.29}$$

The open circuit voltage of a MJ cell is taken to be equal to the sum of the open circuit voltages of each junction.

$$V_{oc} = \sum V_{oc}(i) \tag{3.30}$$

$i = 1, 2 \ldots n$, n is number of junction incorporated in the tandem cell.

3.4.3 Depletion Width

For a typical p-n junction, the contact potential, V_0 is

$$V_o = \frac{kT}{q} \ln \frac{N_a N_d}{n_i^2} \tag{3.31}$$

and the depletion layer width, W is

$$W = \left[\frac{2\varepsilon V_o}{q}\left(\frac{1}{N_a} + \frac{1}{N_d}\right)\right]^{1/2} \tag{3.32}$$

where ε is dielectric constant.

The width of the depletion layer in the n and p type materials are x_{no} and x_{po}.

$$x_{no} = \left\{\frac{2\varepsilon V_o}{q}\left[\frac{N_a}{N_a(N_a + N_d)}\right]\right\}^{1/2} \tag{3.33}$$

$$x_{po} = \left\{\frac{2\varepsilon V_o}{q}\left[\frac{N_d}{N_d(N_a + N_d)}\right]\right\}^{1/2} \tag{3.34}$$

3.4.4 Efficiency

The efficiency of the tandem cell is given by

$$\eta = \frac{J_m V_m}{\Phi_0} \tag{3.35}$$

$$FF = \frac{J_m V_m}{J_{Ph} V_{oc}} \tag{3.36}$$

$$\eta = \frac{J_{ph} V_{oc} FF}{\Phi_0} \tag{3.37}$$

where,

FF = 0.85 has been considered throughout the thesis and Φ_0 is the incident irradiance per unit area in mW/cm^2 whose value is taken form Ref. [26], $\Phi_0 = 96.366$ mW/cm^2.

CHAPTER 4

Performance of In$_x$Ga$_{1-x}$N-based MJ Solar Cells

4.1. Introduction

The design and performance of In$_x$Ga$_{1-x}$N multijunction (MJ) solar cell comprising different number of junctions have been investigated theoretically. The simulation model for the design and performance evolution is based on the theory discussed in the previous chapter. In this chapter, the performances of In$_x$Ga$_{1-x}$N-based MJ solar cells have been shown. For efficiency maximization, the optimum band gap, short-circuit current density and open-circuit voltage are calculated as a function of junctions number of the cell. The current and lattice mismatch at the interfaces of the different junctions have been investigated. The effect of different parameters such as surface recombination velocity, minority carrier life time, emitter thickness and doping density of carriers on the efficiency as well as on the open circuit voltage and short circuit current density have been analyzed for n-p MJ solar cells. The performances of p-n MJ solar cells have also been evaluated. In the entire calculations the n and p regions of the cell are considered as emitter and base, respectively, unless otherwise specified.

4.2 Performance of MJ Solar Cells

The most important drawback of converting solar energy directly to electrical form is its low conversion efficiency for single junction solar cell. In these works the efficiency has been maximized using the MJ approach. Figures 4.1–4.3 show short-circuit current density J$_{SC}$, open-circuit voltage, V$_{OC}$, and conversion efficiency, η, of the InGaN-based MJ solar cells without and with considering the effect of depletion width. The short-circuit current density, J$_{SC}$, without and with considering depletion width decreases with increase in junction number due to the division of the total number of photons between the junctions as shown in Fig. 4.1 (a) and 4.1 (b), respectively. The value of J$_{SC}$ is found to be varied from 30.69 to 6.90 (mA/cm^2) and 31.15 to 6.95 (mA/cm^2) without and with considering depletion width, respectively, for single to eight junction. The constituent components of J$_{SC}$ in the n-region, J$_p$, p-region, J$_n$, and depletion region, J$_w$, are also shown in Fig. 4.1 (b). Similar variation for the open-circuit voltage, V$_{OC}$, is shown in Fig. 4.2. It is found that the V$_{OC}$ increases with increase in junction number, because the total V$_{OC}$ of a cell is the sum of all junction's V$_{OC}$. The value of V$_{OC}$ is found to be varied from 0.898 to 7.389 V for increasing junction number up to eight when depletion width is not considered. However, the V$_{OC}$ is found to vary from 0.891 to 7.387 V for taking into account of
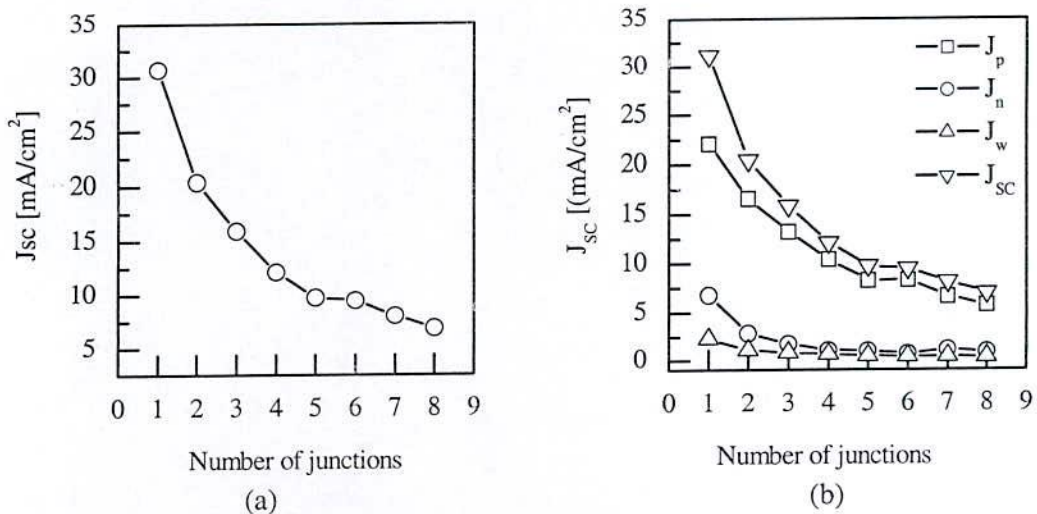
Fig. 4.1 Variation of the short-circuit current density, J$_{SC}$, for MJ solar cells considering a) without depletion width   b) with depletion width.
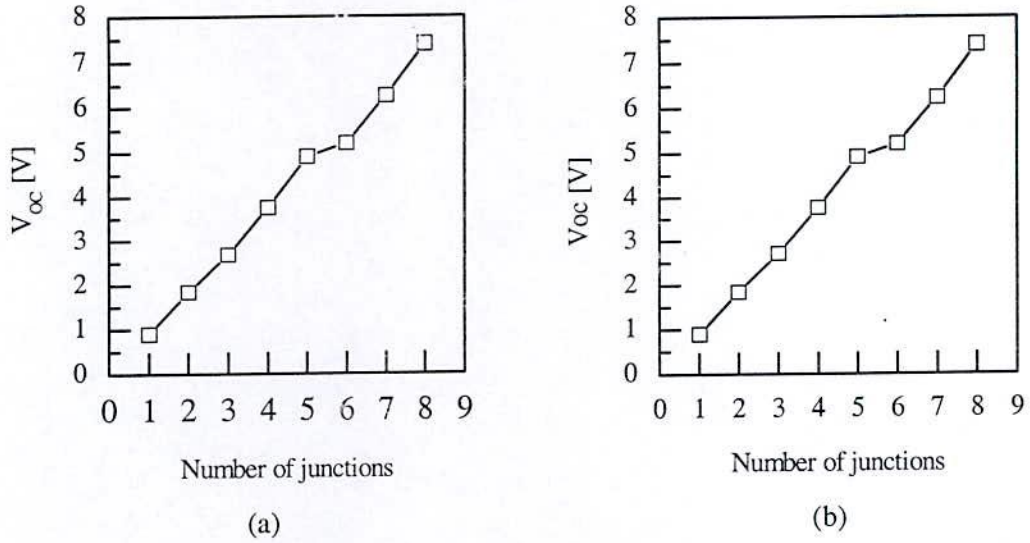
Fig. 4.2 Variation of the open circuit voltage, V$_{OC}$, with the number of junctions considering a) without depletion width   b) with depletion width.
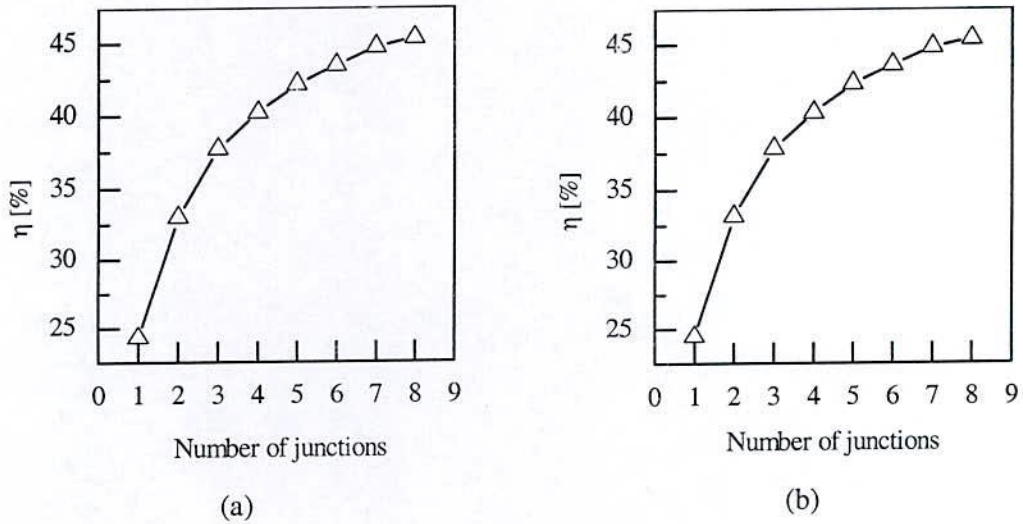
Fig. 4.3 Variation of efficiency, η, with number of junctions considering a) without depletion width   b) with depletion width.

the depletion width effect. The Variation of efficiency, η, as a function of junction number is shown in Fig. 4.3. It is found that the efficiency increases with increase in number of junctions because of the optimization of J$_{SC}$ and V$_{OC}$. The value of η is found to be varied from 24.32 to 45.28 % when depletion width is not considered and 24.49 to 45.35 % when depletion width is considered for single to eight junctions. It is

found that the change in efficiency is not significant if the depletion width is taken into consideration. However, it is important to consider the effect of depletion width on efficiency for getting accurate results. The values of short-circuit current density, J$_{SC}$, open-circuit voltage, V$_{OC}$, and conversion efficiency, η, with the variation of junctions number of a cell without and with considering depletion width are also shown in table 4.1.

Table 4.1: Simulated results of short circuit current density, open circuit voltage and efficiency of In$_x$Ga$_{1-x}$N-based solar cells up to eight junctions.

Number of Junction	Without depletion width			With depletion width		
	J$_{SC}$ (mA/cm^2)	V$_{OC}$ (V)	Efficiency (%)	J$_{SC}$ (mA/cm^2)	V$_{OC}$ (V)	Efficiency (%)
1	30.69	0.898	24.32	31.15	0.891	24.49
2	20.37	1.837	33.01	20.47	1.837	33.17
3	15.94	2.683	37.73	15.88	2.701	37.87
4	12.14	3.752	40.21	12.16	3.752	40.32
5	9.76	4.894	42.19	9.79	4.895	42.29
6	9.42	5.192	43.46	9.50	5.192	43.56
7	8.04	6.251	44.70	8.14	6.226	44.78
8	6.90	7.389	45.28	6.95	7.389	45.35

4.3 Detailed Simulation Results of MJ Solar Cells

The detail simulation results for efficiency optimization in In$_x$Ga$_{1-x}$N-based MJ solar cells have been shown in table 4.2 to table 4.3. The band gap energy, short circuit current density, open circuit voltage, current mismatch, In fraction for In$_x$Ga$_{1-x}$N alloys, lattice mismatch and emitter thickness are shown for each junction of a cell.

Table 4.2: Energy gap, short circuit current density, open circuit voltage, emitter thickness and In composition are calculated for single junction In$_x$Ga$_{1-x}$N cell with total cell thickness 2 μm.

Band gap Eg (eV)	J$_{SC}$ (mA/cm^2)	V$_{OC}$ (V)	In fraction for In$_x$Ga$_{1-x}$N alloys	Emitter thickness (μm)
1.381	31.15	0.8911	0.517	0.3

Table 4.3: Energy gap, short circuit current density, current mismatch, open circuit voltage, lattice mismatch, emitter thickness and In composition are calculated for In$_x$Ga$_{1-x}$N tandem cell with total thickness of each junction 2 μm.

No. of Junctions	Band gap Eg (eV)	J$_{SC}$ (mA/cm^2)	Current mismatch (%)	V$_{OC}$ (V)	In fraction for In$_x$Ga$_{1-x}$N alloys	Lattice mismatch (%)	Emitter thick-ness (μm)
2	1.719	20.47	0.098	1.2185	0.4		0.3
	1.12	20.45	0.0	0.6188	0.628	2.56	0.32
3	1.899	15.89	0.063	1.392	0.346		0.3
	1.372	15.88	0.0	0.8645	0.52	1.98	0.32
	0.952	15.90	0.13	0.4449	0.72	2.54	0.31
4	2.074	12.18	0.16	1.5596	0.298		0.3
	1.586	12.16	0.0	1.0722	0.443·	1.66	0.32
	1.221	12.18	0.16	0.7072	0.582	1.56	0.32
	0.927	12.18	0.16	0.4132	0.736	1.70	0.31
5	2.21	9.79	0.0	1.6904	0.262		0.3
	1.757	9.79	0.0	1.2371	0.389	1.46	0.32
	1.44	9.79	0.0	0.9203	0.494	1.19	0.31
	1.166	9.79	0.0	0.6465	0.606	1.26	0.32
	0.92	9.80	0.1	0.4003	0.741	1.5	0.31
6	2.228	9.51	0.1	1.7075	0.257		0.3
	1.778	9.52	0.21	1.2578	0.382	1.38	0.32
	1.462	9.50	0.0	0.9416	0.486	1.18	0.33
	1.19	9.52	0.21	0.6692	0.596	1.23	0.32
	0.957	9.52	0.21	0.4368	0.717	1.34	0.31
	0.7	9.51	0.1	0.1795	1	3.15	0.2
7	2.32	8.15	0.12	1.7929	0.234		0.3
	1.888	8.16	0.24	1.3604	0.35	1.34	0.32
	1.588	8.14	0.0	1.0608	0.443	1.06	0.32
	1.355	8.15	0.12	0.8263	0.527	0.95	0.32
	1.135	8.15	0.12	0.6077	0.621	10.5	0.32
	0.932	8.16	0.24	0.4011	0.733	1.24	0.31
	0.706	8.15	0.12	0.1772	0.977	2.63	0.32
8	2.407	6.96	0.14	1.8786	0.231		0.3
	1.992	6.96	0.14	1.4636	0.32	1.03	0.31
	1.711	6.97	0.29	1.1823	0.403	0.95	0.33
	1.484	6.95	0.0	0.9554	0.479	0.87	0.31
	1.265	6.96	0.14	0.7363	0.563	0.94	0.32
	1.095	6.96	0.14	0.5667	0.64	0.86	0.32
	0.935	6.95	0.0	0.4063	0.731	1.0	0.3
	0.729	6.96	0.14	0.2001	0.926	2.11	0.18

4.4 Effect of Band gap Optimization

Band gap optimization has a positive effect on the efficiency of the MJ solar cell. The variation of efficiency with the bottom junction band gap energy is shown in Fig. 4.4. The optimum bottom junction band gap energies are evaluated corresponding to the maximum efficiency. The optimum band gap energies are found to be 1.381 eV, 1.12
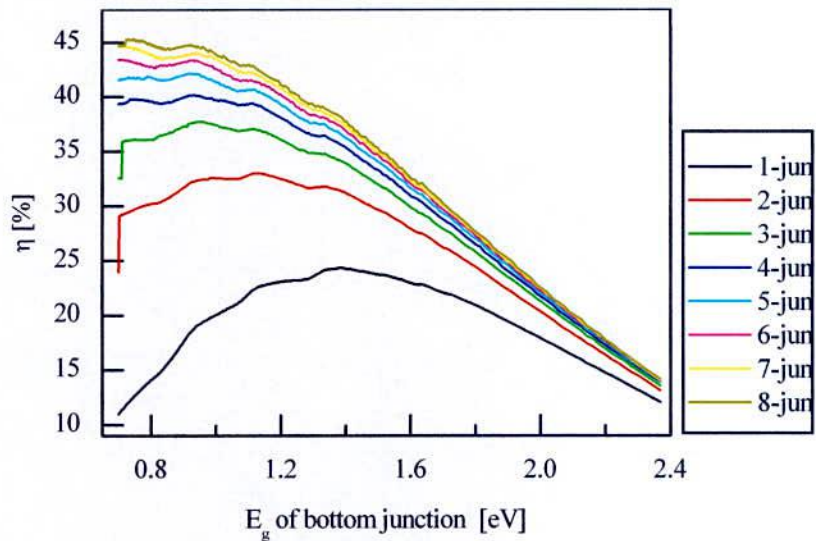

Fig. 4.4 Optimization of efficiency with the variation of bottom junction band gap energy.
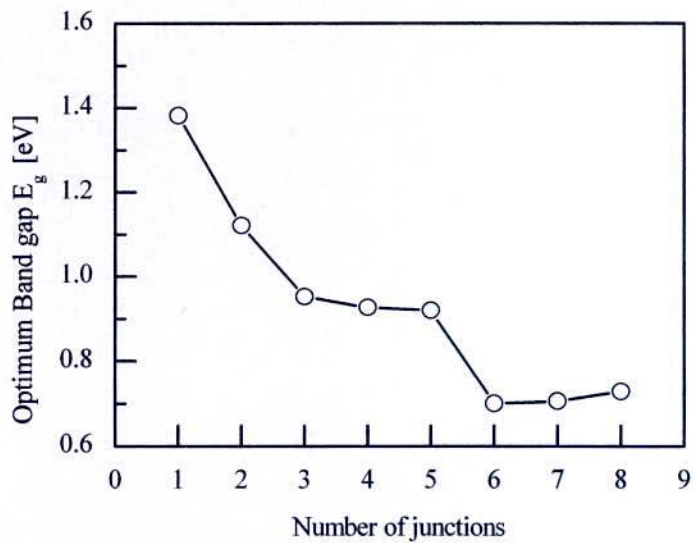

Fig. 4.5 Optimum band gap energy of bottom junction up to eight junction solar cell.

eV, 0.952 eV, 0.927 eV, 0.92 eV, 0.7eV. 0.706 eV and 0.729 eV, respectively, for single to eight junctions cell. Figure 4.5 shows the plot of optimum bottom junction band gap energies as a function of junction number. It is found in Fig. 4.5 that the band gap energy of the bottom junction decreases with increasing the junction number. However, after six junctions the band gap energies are found to be increased with junction number.

4.5 Current Mismatch

The current flows through a MJ solar cell from the top to the bottom junction is the minimum photocurrent generated in each cell. Therefore, the current passing through each layer should be the same. For maximum efficiency, the cell must be designed so that each layer produces the same current which reduces the loss. Current mismatch in MJ solar cell is the difference of current of the junction. For better performance, it should be as less as possible. Theoretically, the current mismatch between the junction's photocurrent densities should not exceed 5%. In this work, it is kept within 0.29 %. The minimum to maximum current mismatch for different junctions is shown in Fig. 4.6. As the junction number increases, the current mismatch of the MJ solar cell increases. Here the photocurrent of each junction is adjusted by tuning the thickness of the emitter of each cell to match the current.
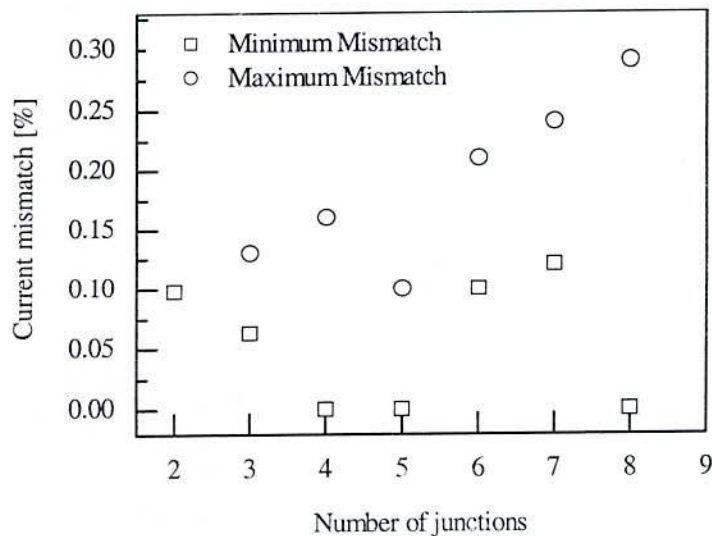

Fig. 4.6 Variation of current mismatch with number of junctions.

4.6 Lattice Mismatch

The lattice constant is a measure of the distance between atom locations in a unit cell of crystal. It is extremely desirable to match the lattice constants of the various layers. Mismatch in the crystal lattice constants creates defects or dislocations in the lattice where recombination centers can occur. Recombination results in the loss of photogenerated minority carriers (e.g., electrons drop from the conduction band back into the valence band) and significantly degrades the photovoltaic quality of the device. Such effects will decrease the open-circuit voltage, short-circuit current density and fill factor, which represent the relationship or balance between current and voltage for effective power output. In this modeling the lattice constants of ternary alloys are predicted according to Vegard's law [27]. Lattice mismatch in MJ
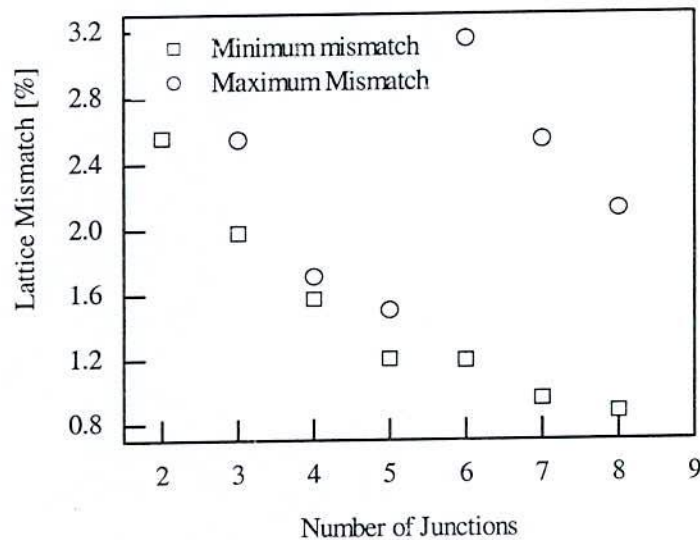
Fig. 4.7 Variation of lattice mismatch with junction number.

solar cell is the difference of lattice constant of two adjacent junctions. For better performance it should be as minimum as possible. The lattice mismatch (minimum to maximum) between the junctions in the cell is shown in Fig. 4.7. It is noticeable that with increasing the junction number, the minimum lattice mismatch between the junctions decreases. Because increasing number of junctions the difference in Indium fraction between two adjacent junctions decreases. For single junction solar cell there is no lattice mismatch as only one junction is used. For two junction solar cell, there is only one lattice mismatch as there is only one interface between the junctions and that

is 2.56%. For three junction solar cell, it is found from 1.98% to 2.54%. For four junction solar cell, it is found between 1.56% and 1.70%. Lattice mismatch for five junction solar cell is between 1.19% and 1.5%. For six junction solar cell, there is large change in lattice mismatch (from 1.18% to 3.15%). Because deference between band gap of 5th and 6th junction of this solar cell is much as compared to other junctions (table 4.3). The minimum to maximum mismatch for seven and eight junctions is 0.95% to 2.63% and 0.86% to 2.11%, respectively.

4.7 Conversion Efficiency of *n-p* MJ Solar cells

4.7.1 Effect of Surface Recombination Velocity

Surface recombination velocity, S, is an important property of optoelectronic materials. As the size of optoelectronic devices becomes smaller, surface effects begin to influence their performance. It has a substantial impact on the performance of solar cells. Surface recombination velocity of carriers imposes limitations on the efficiency of MJ solar cells and other devices that require the size of the active region to be comparable to the minority carrier diffusion length. The efficiency of the solar cell is significantly lowered by increasing S. The S generally increases with increasing doping density. The surface recombination velocity of direct band gap semiconductor, such as GaAs, InP, GaN, InN etc. is very high. Suitable doping density has been devised for InN device which help a great to reduce the surface recombination velocity and improve the efficiency of In$_x$Ga$_{1-x}$N-based MJ solar cells.

Figures 4.8–4.10 shows dependency of short-circuit current density, J$_{SC}$, open-circuit voltage, V$_{OC}$, and conversion efficiency, η, of the In$_x$Ga$_{1-x}$N-based MJ solar cells with the surface recombination velocity. The J$_{SC}$, V$_{OC}$, and η decrease with increasing surface recombination velocity of each junction. The most significant effect of surface recombination velocity is observed on J$_{SC}$. Because increasing the recombination rate of the carrier reduces the J$_{SC}$. Therefore, η decreases with increasing surface recombination velocity of the In$_x$Ga$_{1-x}$N-based MJ solar cells as indicated in Fig. 4.10.
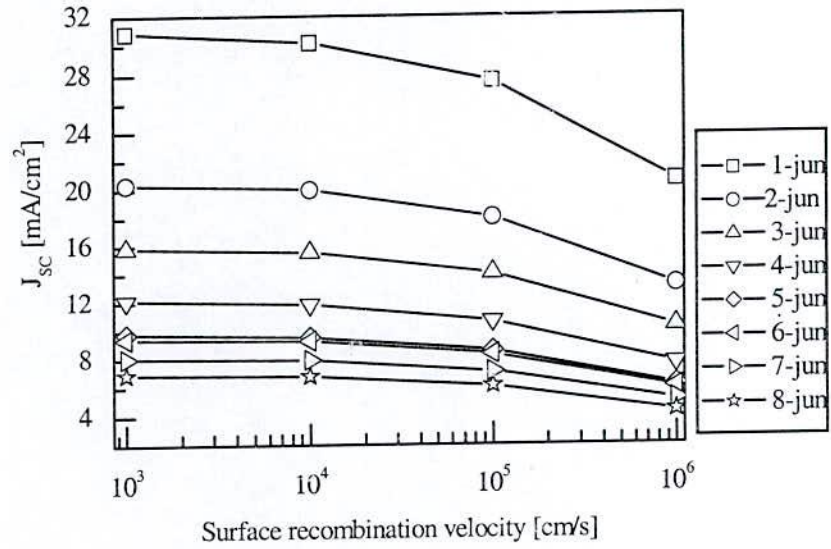
Fig. 4.8 Variation of the short circuit current density, J$_{SC}$ with surface recombination velocity up to 8-junction.
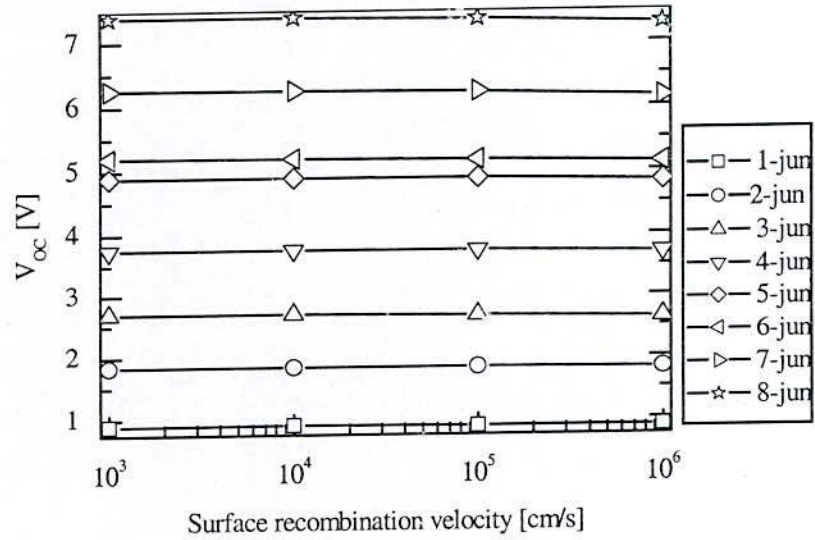

Fig. 4.9 Variation of the open circuit voltage with surface recombination velocity up to 8-junction.
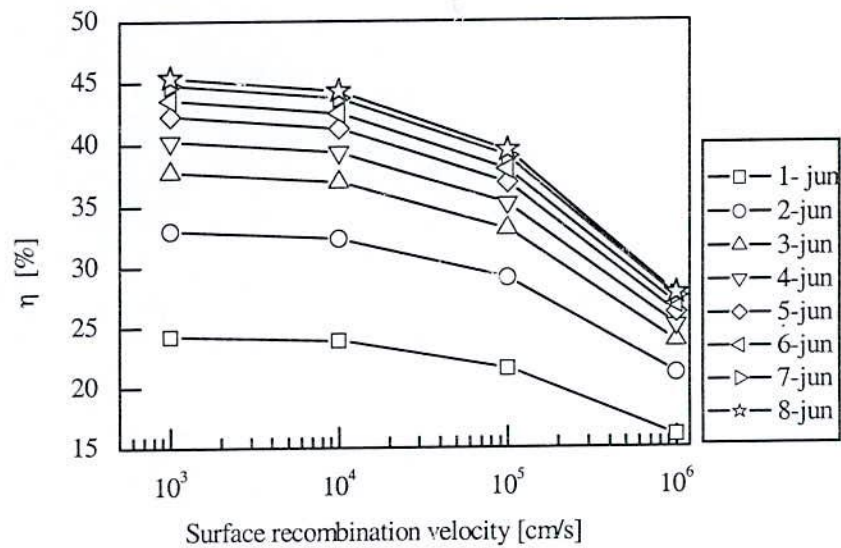
Fig. 4.10 Variation of the conversion efficiency, η, with surface recombination velocity up to 8-junction.

4.7.2 Effect of Minority Carrier Life Time

Minority carrier lifetime is the most critical parameter in determining the performance of the MJ solar cells. This parameter depends strongly on manufacturing techniques. If the crystal quality improves i.e. defect density decreases, the minority carrier lifetime becomes long. Using the room temperature photoluminescence intensity as a indirect measure of minority carrier lifetime, it is shown that $In_xGa_{1-x}N$ retains its optoelectronic properties at radiation damage doses at least 2 orders of magnitude higher than the damage thresholds of the materials (GaAs and GaInP) currently used in high efficiency MJ cells [28]. The presence of an electron-rich surface layer in InN and $In_{1-x}Ga_xN$ ($0 < x < 0.63$) is investigated; it is shown that the minority carrier lifetime is a less significant effect at large x [28]. Diffusion length depends on the minority carrier lifetime. The electron diffusion length is quite short and is usually less than the hole diffusion length. Figures 4.11– 4.13 show the dependency of J_{SC}, V_{OC} and η with minority carrier lifetime of base (base diffusion length) of the $In_xGa_{1-x}N$-based MJ solar cells. The J_{SC}, V_{OC} and η increases with the increase in the minority carrier lifetime of base of each junction. There is most significant effect of the minority carrier lifetime of base on short circuit current density. Due to increase
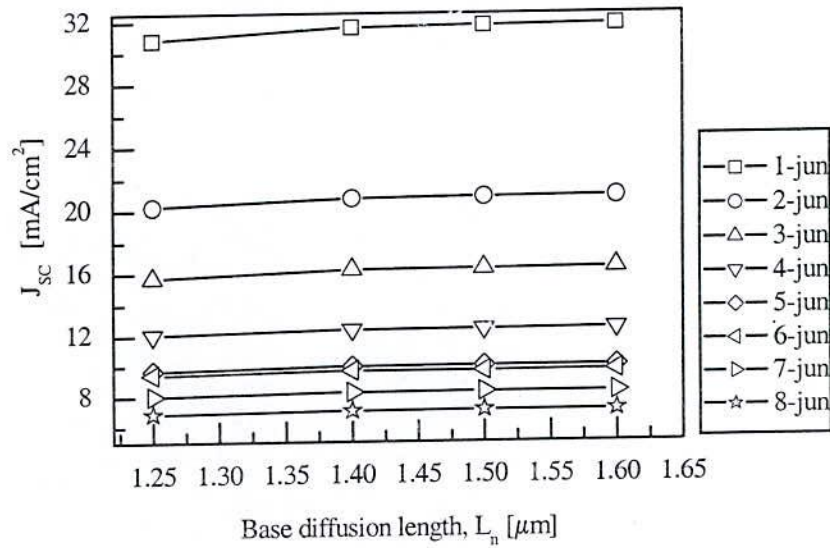
Fig. 4.11 Variation of the short circuit current density, J$_{SC}$, with base diffusion length up to 8-junction.
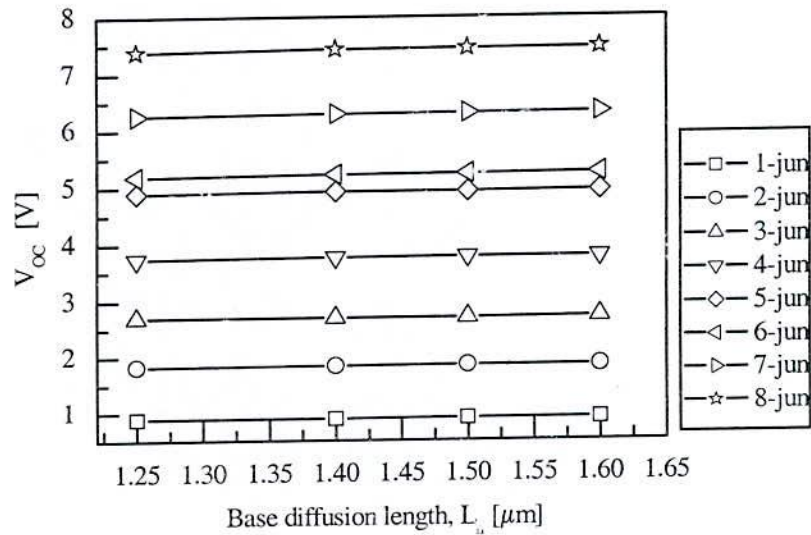
Fig. 4.12 Variation of the open circuit voltage, V$_{OC}$, with base diffusion length up to 8-junction.

the lifetime (diffusion length) of photogenerated carriers, the photocurrent increases. Therefore, efficiency increases with increasing the base minority carrier lifetime of the In$_x$Ga$_{1-x}$N-based MJ solar cells.
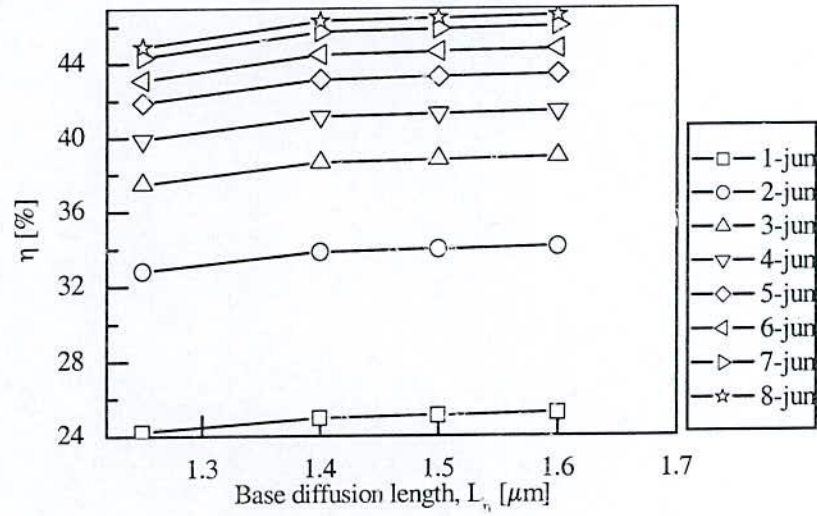
Fig. 4.13 Variation of conversion efficiency, η, with base diffusion length up to 8-junction.
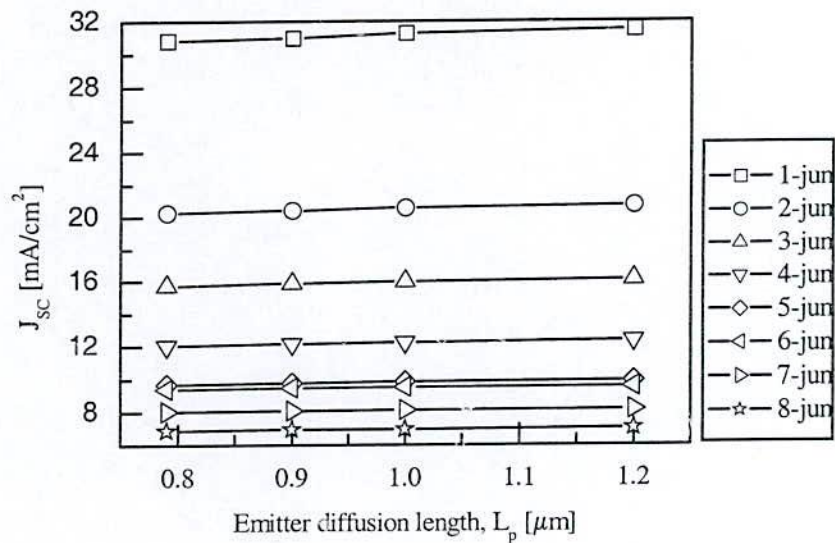
Fig. 4.14 Variation of the short circuit current density, J$_{SC}$, with emitter diffusion length up to 8-junction.

Similar results are shown in Fig. 4.14 – 4.16 with emitter minority carrier lifetime (emitter diffusion length). The short circuit current density, J$_{SC}$, open-circuit voltage, V$_{OC}$, and conversion efficiency, η, increases with increasing minority carrier lifetime in the emitter region of each junction. The emitter minority carrier lifetime plays an

important role on short circuit current density. Due to increase the lifetime (diffusion length) of the photogenerated carriers, the photocurrent increases. Therefore, efficiency increases with increase in the emitter minority carrier lifetime of the In$_x$Ga$_{1-x}$N-based MJ solar cells.
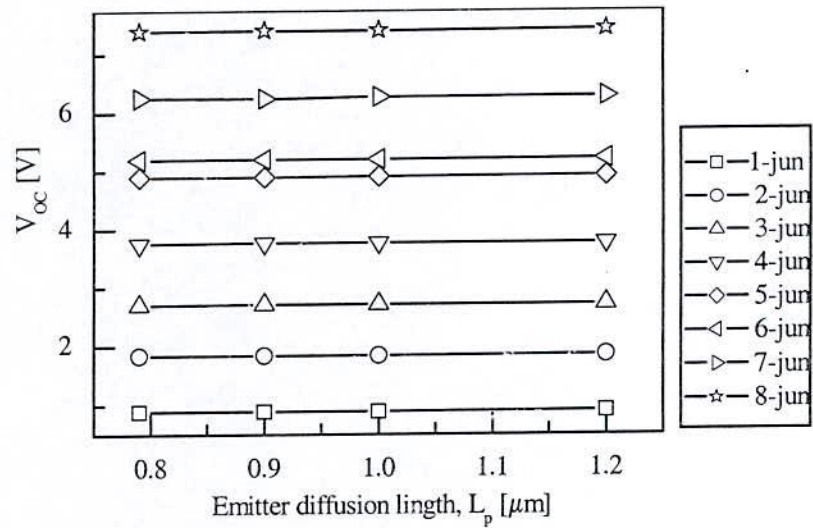
Fig. 4.15 Variation of the open circuit voltage, V$_{OC}$, with emitter diffusion length up to 8-junction.
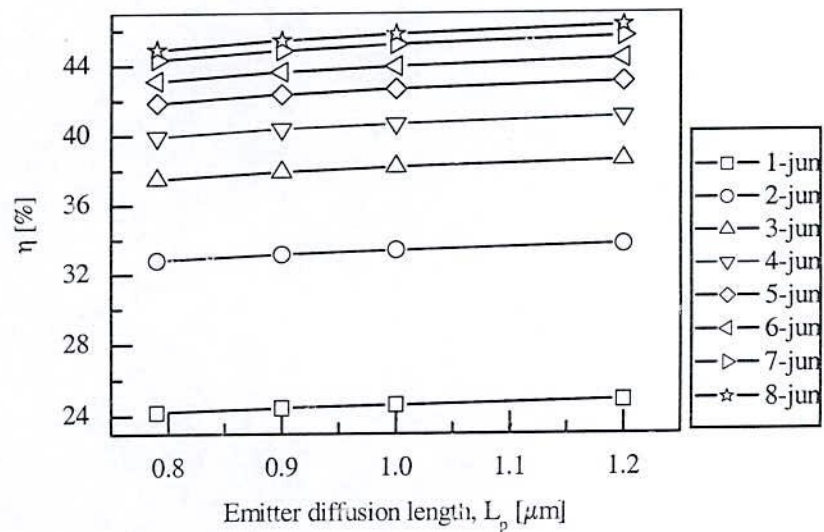
Fig. 4.16 Variation of conversion efficiency, η, with emitter diffusion length up to 8-junction.

4.7.3 Effect of Emitter Thickness

Thickness of the emitter plays a significant role on efficiency. Figures 4.17–4.19 show the effect of emitter thickness on J$_{SC}$, V$_{OC}$ and η of the In$_x$Ga$_{1-x}$N-based MJ solar cells. The variation of J$_{SC}$ is shown with the variation of emitter thickness in Fig. 4.17 where J$_{SC}$ is found to be decreased with increase in emitter thickness. The variation of
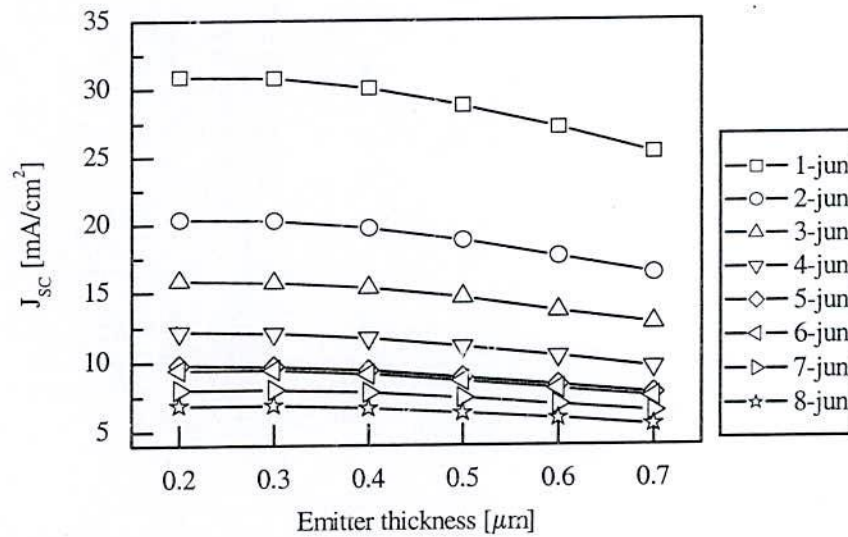
Fig. 4.17 Variation of short circuit current density, J$_{SC}$, with emitter thickness up to 8-junction.
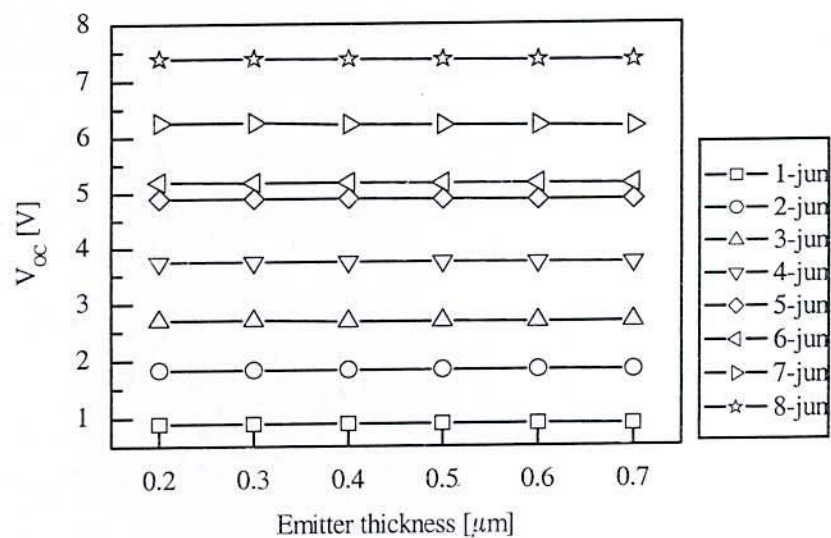
Fig. 4.18 Variation of open circuit voltage, V$_{OC}$, with emitter thickness up to 8-junction.

53
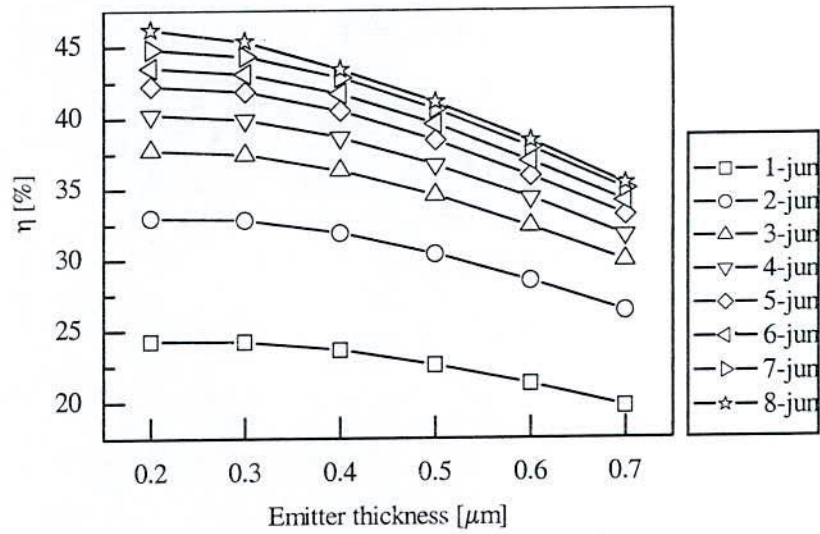
Fig. 4.19 Variation of efficiency, η, with emitter thickness up to 8-junction.

V$_{OC}$ is shown in Fig. 4.18, where changes of V$_{OC}$ are almost negligible with emitter thickness of the individual cell. However, for a particular emitter thickness, the values of V$_{OC}$ are found to be changed significantly if the junction of the cell is increased. Figure 4.19 shows that the η decreases with increasing the thickness of emitter of each junction. It is found that for a particular emitter thickness, change in efficiency is larger for a cell with more number of junctions than a cell with less number of junctions. This demonstrates that the change in efficiency becomes saturated with increasing junction number. It may be suggested from the results in Fig. 4.19 that the thickness should be kept as less as possible in order to get higher efficiency. In this work the emitter thickness of first junction is considered 0.3µm. The thickness of the other junctions is determined to minimize the current mismatch. Decrease of emitter thickness below 0.2µm increases the current mismatch between different cells.

4.7.4 Effect of Donor and Acceptor Concentration

The doping density plays an important role on efficiency. It is well known that radiative lifetime decreases with increasing doping level. Consequently, radiative recombination becomes dominant compared to nonradiative recombination. The variation of efficiency with different carrier concentrations is shown in Fig. 4.20 where the efficiency is found to increase with increasing carrier concentration. It is

well established that if the doping concentration is increased the reverse saturation current is decreased. As a result efficiency is increased due to increase of V$_{OC}$.
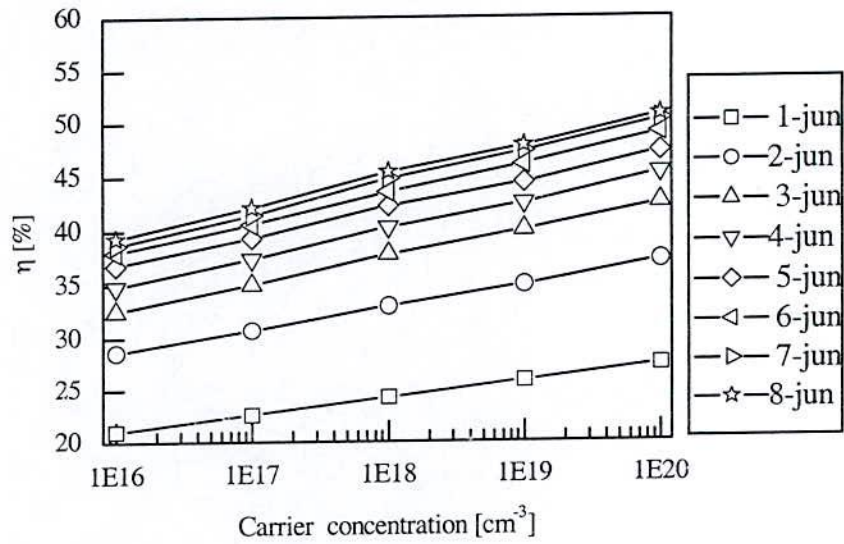
Fig. 4.20 Variation of efficiency, η, with carrier concentration up to 8-junction considering equal N$_a$ and N$_d$.
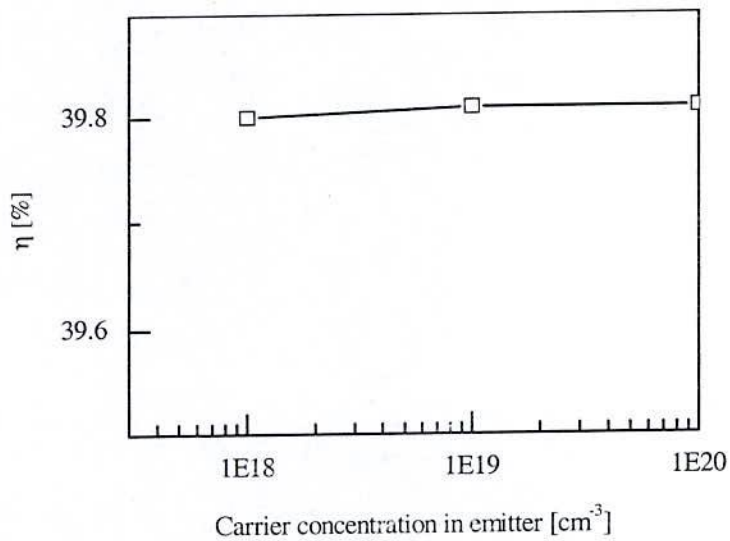
Fig. 4.21 Variation of efficiency, η, with emitter carrier concentration of 8-junction n$^+$- p cell.
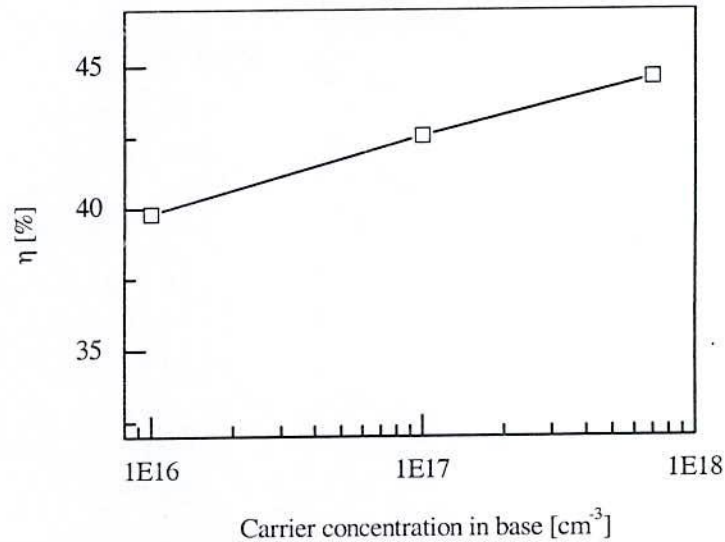
Fig. 4.22 Variation of efficiency, η, with base carrier concentration of 8-junction n$^+$ - p cell.

The variation of efficiency with emitter carrier concentration of 8-junction n$^+$.p cell is shown in Fig. 4.21. The base carrier concentration is considered 1×10^{16} (cm^{-3}) in this calculation. The η is found to be nearly constant with emitter carrier concentration. The variation of efficiency with base carrier concentration of 8-junction n$^+$. p cell is shown in Fig. 4.22. The emitter carrier concentration is considered 1×10^{18} (cm^{-3}) in this calculation. The efficiency is found to be increased with the increasing base carrier concentration.

4.8 Conversion Efficiency of p-n MJ Solar Cells

The previous sections described the performances of In$_x$Ga$_{1-x}$N-based MJ solar cells where emitter is considered as n type and base as p type, i.e., *n* on *p*. In order to examine the performance and details understanding the InGaN-based MJ solar cells where emitter is considered as *p* and base as *n* have also been studied. There is no significant change in the performances between *n-p* and *p-n* cells. Figure 4.23 shows the short-circuit current density, J$_{SC}$, open-circuit voltage, V$_{OC}$, and conversion efficiency, η, with the variation of number of junction of the proposed In$_x$Ga$_{1-x}$N-based MJ *p-n* solar cells. The J$_{SC}$ decreases with increase in junction number. The value of J$_{SC}$ is found to be varied from 30.36 to 6.90 (mA/cm^2) for single to eight junctions, respectively. The open circuit voltage, V$_{OC}$, is found to be increased from
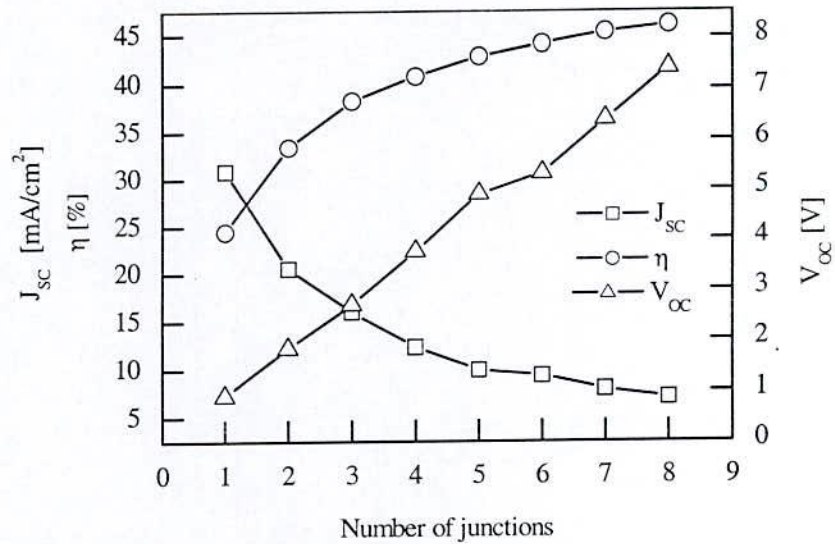
Fig. 4.23 Variation of the open-circuit voltage short-circuits current density and efficiency with number of junctions in the p-n cell.

0.898 to 7.389 (V) with increase in number of junction from single to eight. Finally the efficiency is varied from 24.05% to 45.32% with increase in junction number from single to eight.
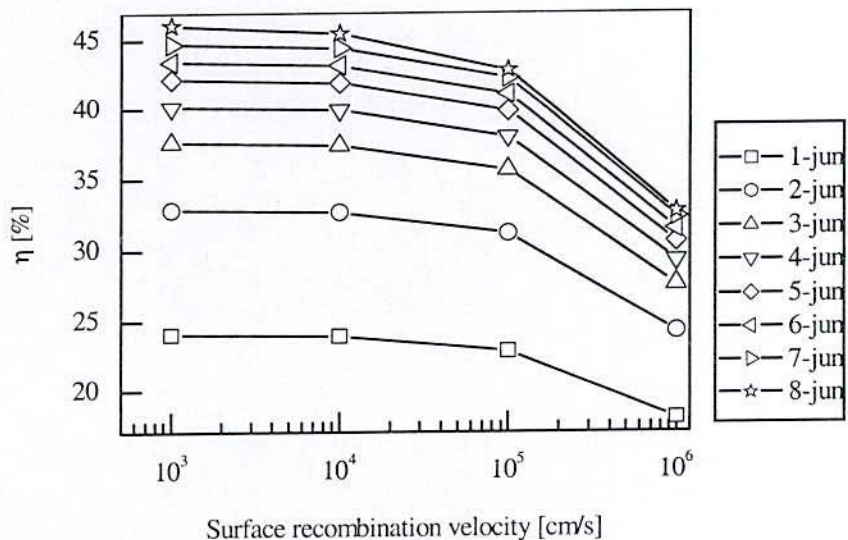
Fig. 4.24 Variation of the efficiency, η, with surface recombination velocity up to 8-junction in the p-n cell.

Figure 4.24 shows the surface recombination velocity dependences of conversion efficiency, η, of the In$_x$Ga$_{1-x}$N-based MJ solar cells. The efficiency decreases with increase in surface recombination velocity of the In$_x$Ga$_{1-x}$N-based MJ solar cells. The variation of efficiency with emitter diffusion length is shown in Fig. 4.25 of the InGaN-based MJ solar cells. The efficiency increases with increase in emitter diffusion length.
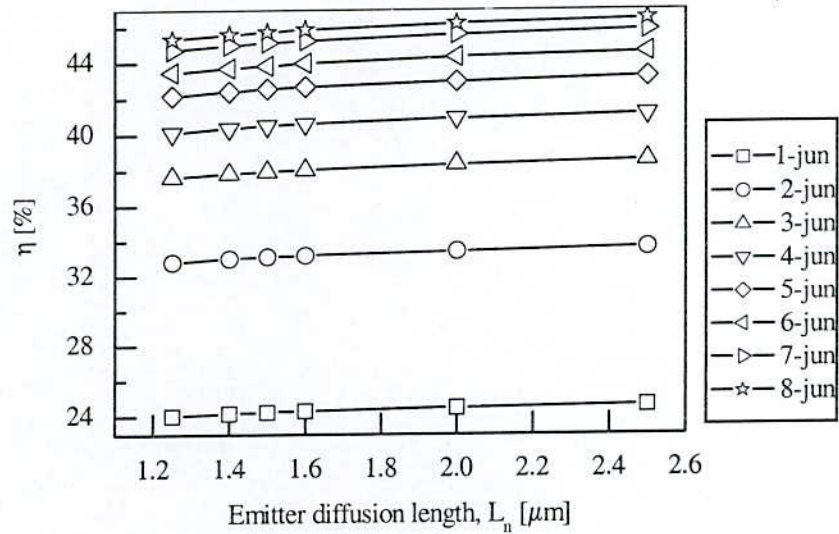
Fig. 4.25 Variation of the efficiency with emitter diffusion length up to 8-junction p-n cell.
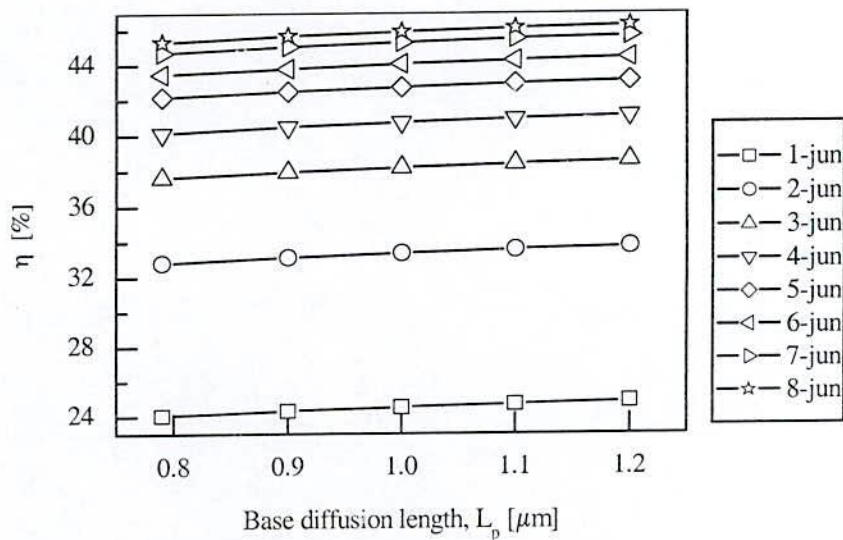
Fig. 4.26 Variation of the efficiency with base diffusion length up to 8-junction in the p-n cell.
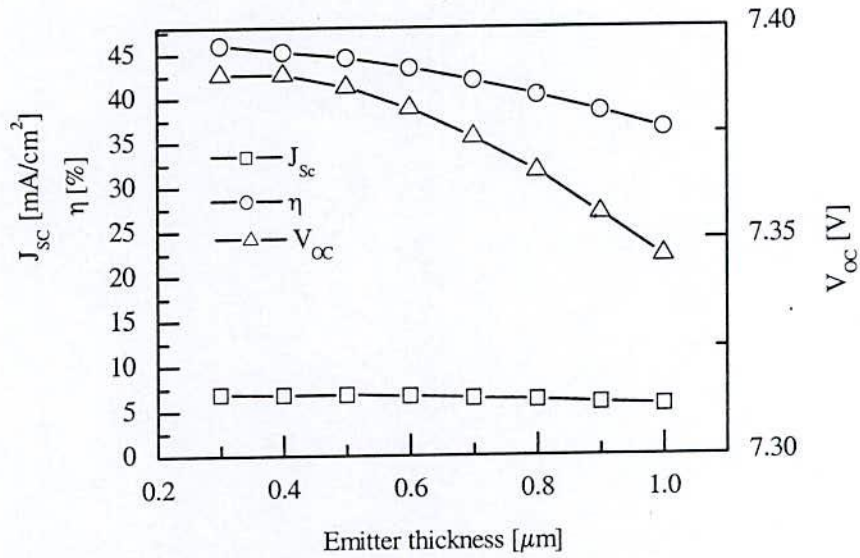
Fig. 4.27 Variation of the short circuit current, open circuit voltage and efficiency with emitter thickness of a 8-junction p-n cell.
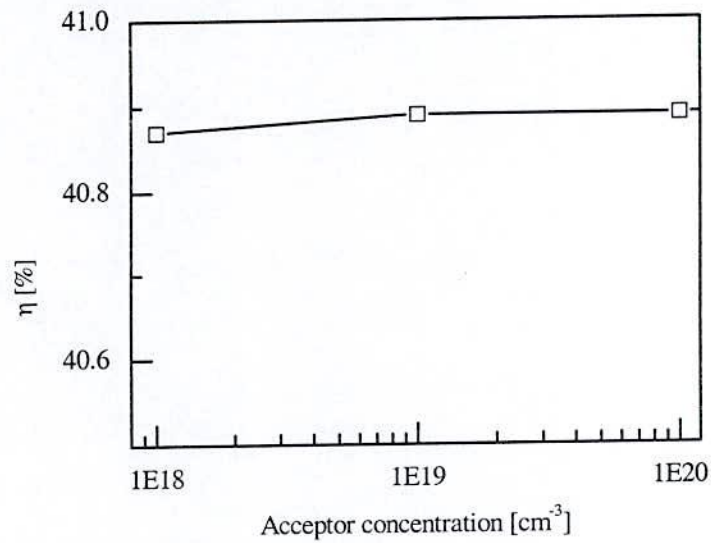
Fig. 4.28 Variation of efficiency with emitter concentration of 8-junction p$^+$. n solar cell.

Figure 4.26 shows the variation of efficiency with base diffusion length of the InGaN-based MJ solar cells. The efficiency increases with increase in base diffusion length. Figure 4.27 shows that the short circuit current, open circuit voltage and efficiency decreases with increasing the thickness of emitter of each junction. The efficiency increases with decrease in emitter thickness. The variation of efficiency of a p$^+$. n cell

is shown in Fig. 4.28. The efficiency increases with the increase in emitter carrier concentration.

The values of short-circuit current density, J$_{SC}$, open-circuit voltage, V$_{OC}$, and conversion efficiency, η, with the variation of junction number of a *n-p* and *p-n* cell are also shown in table 4.3.

Table 4.4: Comparative simulated results of n-p and p-n In$_x$Ga$_{1-x}$N-based solar cells up to eight junctions.

Number of Junction	n-p Junction			p-n Junction		
	J$_{SC}$ (mA/cm^2)	V$_{OC}$ (V)	Efficiency (%)	J$_{SC}$ (mA/cm^2)	V$_{OC}$ (V)	Efficiency (%)
1	31.15	0.891	24.49	30.36	0.898	24.05
2	20.47	1.837	33.17	20.27	1.837	32.83
3	15.88	2.701	37.87	15.79	2.701	37.62
4	12.16	3.752	40.32	12.13	3.752	40.14
5	9.79	4.895	42.29	9.77	4.894	42.16
6	9.50	5.192	43.56	9.40	5.192	43.44
7	8.14	6.226	44.78	8.03	6.251	44.71
8	6.95	7.389	45.35	6.92	7.389	45.32

CHAPTER 5
InGaN Solar Cells with Concentrator

5.1 Introduction

Light concentration is one of the important issues for the development of an advanced PV system using high-efficiency solar cells. High-efficiency multijunction cells, under high-concentration operations, have been investigated for terrestrial application [2, 3]. Also, low-concentration operations with multijunction cells have been investigated for space satellites [4-6]. In order to attain the high efficiency concentrator InGaN-based multijunction solar cell, accurate evaluation under concentrate light, is necessary. However, the accurate measurement and evaluation of cell characteristics under concentrated light are very difficult because of an increase of cell temperature, chromatic aberration and intensity distribution. The chromatic aberration and intensity distribution caused by light concentration with a lens have various influences on multijunction solar cells [29, 30]. Moreover, energy losses due to series resistance caused by the handling of large currents decrease the cell efficiency, and the series resistance is an important factor

of concentrator on InGaN-based multijunction solar cell. The concentrator photovoltaic system and effect of concentrator on efficiency are discussed in this chapter. The performance of multijunction solar cells under concentrator with temperature has been also shown.

5.2 Concentrator Photovoltaic System

The total worldwide solar cell production in the year 2001 was 400 MW, mostly in the form of flat-plate Si solar cells. In the context of world energy consumption, 400 MW is not enough. Moreover, 20 t/MW of silicon is required for solar cells, and the silicon that can be used for solar cells is restricted to 1000 tons per year [31]. Therefore, we will face the problem of a shortage of silicon material for mass production in the future. One way to resolve the problem of cost and shortage of semiconductor materials is to employ concentrator systems, which concentrate sunlight with a lens, thereby increasing the intensity of sunlight striking the solar cell. Figure 5.1 shows a system configuration of concentrator PV system. A concentrator PV system is composed of solar cell, optics such as lens or mirror, and tracker. The primary reason for using concentrators is to decrease the area of solar cell material being used in a system because solar cells are an expensive component of a PV system. Replacing semiconductor solar cell area with lower cost plastic lenses leads to lower overall system cost. For a concentrator module, the solar cell area is a small fraction of the total module area. A concentrator uses relatively inexpensive materials (plastic lenses, metal housings, etc.) to capture a large area of solar energy and focus it onto a small area, where the smaller solar cell resides. Moreover, as a merit of concentrator systems, the conversion efficiency of cell increases. Therefore, we can see that the concentrator systems using super high efficiency multijunction solar cells have great potential as high-performance and low-cost PV systems, even if the cost of the solar cell itself is high.
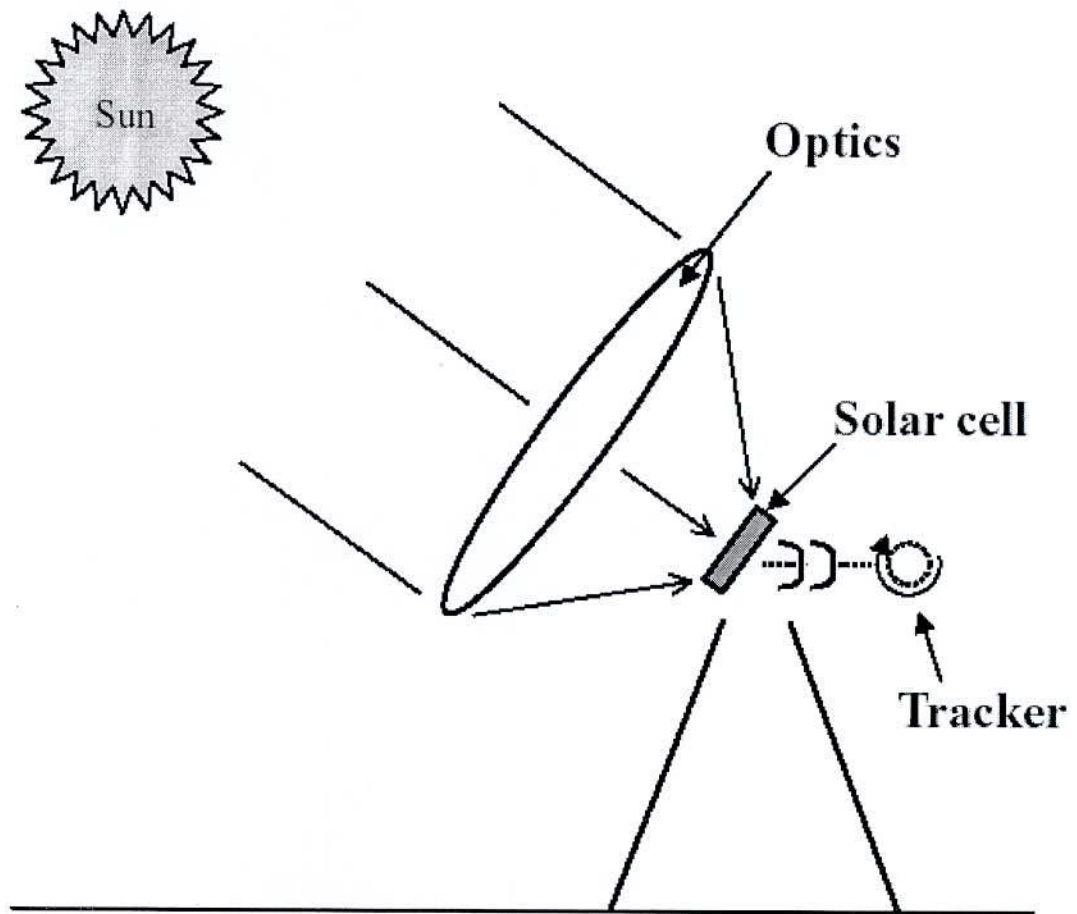
Fig. 5.1 System configuration of concentrator PV system.

5.3 Conversion Efficiency of Concentrator Solar Cell

In order to attain the high efficiency concentrator InGaN-based multijunction solar cell, the evaluation under concentrated light is necessary. High-efficiency InGaN-based multijunction cells, under concentration operations with two suns, have been studied. In this work, concentrator PV system is composed of solar cell with non-imagining Fresnel lens considering as concentrator. The optical efficiency of the proposed non-imagining Fresnel lens is considered as 85% [32]. The effect of concentrator on short-circuit current density, J_{SC}, with the variation of number of junctions is shown in Fig. 5.2. The short-circuit current density, J_{SC}, is found to be varied from 31.15 to 49.32 (mA/cm^2) for single
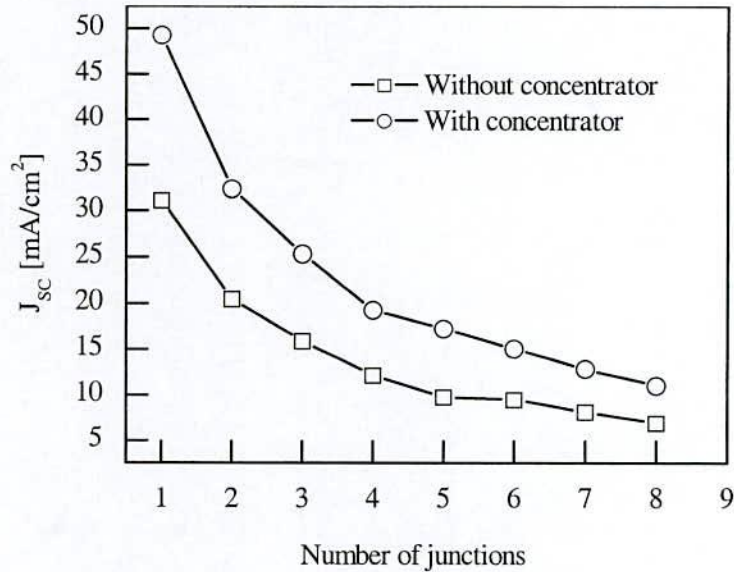
Fig. 5.2 Variation of the short-circuit current density, J_{SC}, with number of junctions in the cells with and without concentrator.

and 6.95 to 11.01 (mA/cm^2) for eight junction, without and with concentrator, respectively. Due to concentrator, more photons absorb in each junction which increase the short circuit current density. Figure 5.3 shows the effect of concentrator on open-circuit voltage, V_{OC}, with the variation of number of junctions. The V_{OC} is found to be varied from 0.891 to 0.903 (V) for single junction and 7.389 to 7.485 (V) for eight junction, without and with concentrator, respectively. The open circuit voltage increases with the increase of the short circuit current of each junction by using concentrator. The effect of concentrator on the efficiency of InGaN-based multijunction solar cell, with variation of number of junctions is shown in Fig. 5.4. The efficiency, η, is found to be varied from 24.49 to 39.28 (%) for single junction and 45.35 to 72.79 (%) for eight junction, without and with concentrator, respectively. These results are in good agreement with the report of Yamaguichi et al. [33].

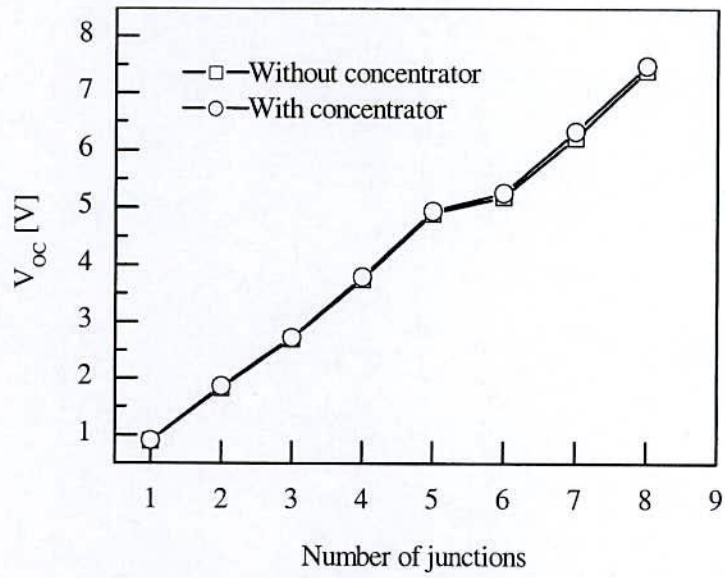**Fig. 5.3** Variation of open circuit voltage, V_{OC}, with number of junctions in the cells with and without concentrator.
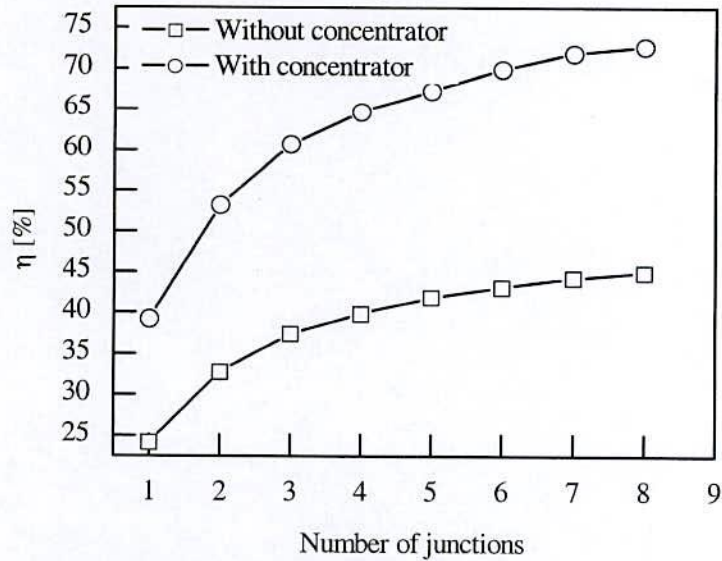

Fig. 5.4 Variation of efficiency, η, with number of junctions in the cells with and without concentrator.

5.4   Effect of Temperature of InGaN-based MJ Solar Cells

It is considered that the temperature of solar cells rises under light concentrating operations. It is true that the cell is exposed by the high-energy flow and is potentially heated to 1400^0C at 500 suns concentration if it is insulated [34]. The conversion efficiency decreases when the temperature of the solar cell rises [35, 36]. Though passive cooling methods with a heat sink [37] or a heat spreader [38] have been favored for cost and reliability purposes, they could not completely suppress the rise of cell temperature. Moreover, since air is a medium, passive cooling is very difficult, especially for space satellites. The temperature characteristics of the InGaN-based multijunction solar cells under concentration have not been evaluated in detail. The temperature dependences characteristics of InGaN-based multijunction solar cells under concentration are calculated. For MJ solar cells, conversion efficiency decreases with increasing temperature, and increases with concentration owing to an increase in short circuit current and open-circuit voltage which are shown in Fig. 5.5-5.7. The temperature dependences of the solar cell's characteristics are calculated in the temperature range from 280^0 to 400^0 K. Figure 5.5 shows the effect on concentrator on the temperature dependence of short circuit current density, J_{SC}. The increase in minority-carrier diffusion length and the shift in optical absorption edge energy with increasing temperature produce a small increase in J_{SC}. An increase in J_{SC} with increasing temperature results from the change in absorption coefficient with temperature which has not considered in this calculation. Fig. 5.6 shows the temperature dependence of V_{OC}. For concentrator and without concentrator, V_{OC} decreased with increasing temperature.
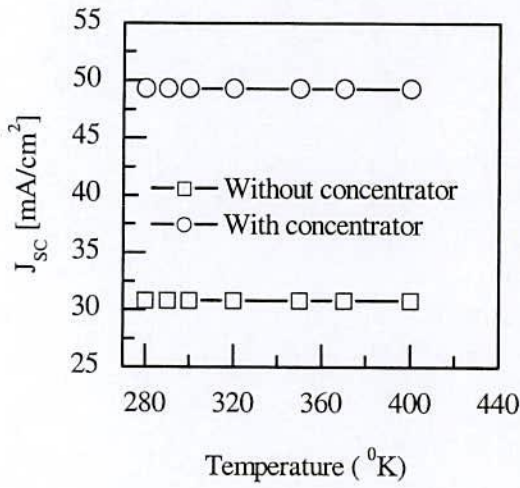
(a) Single junction
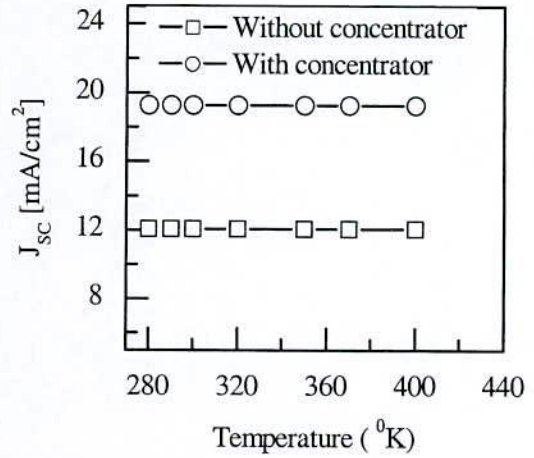
(c) Four junctions
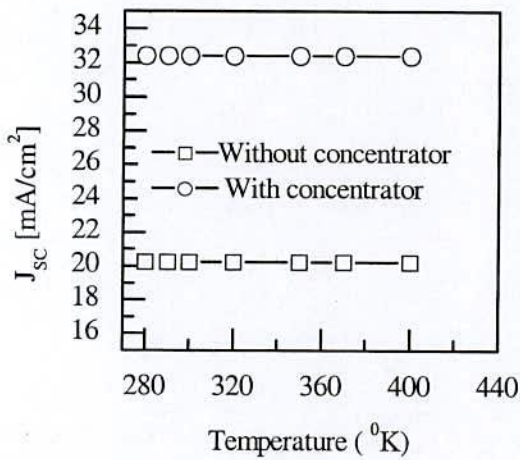
(b) Two junctions
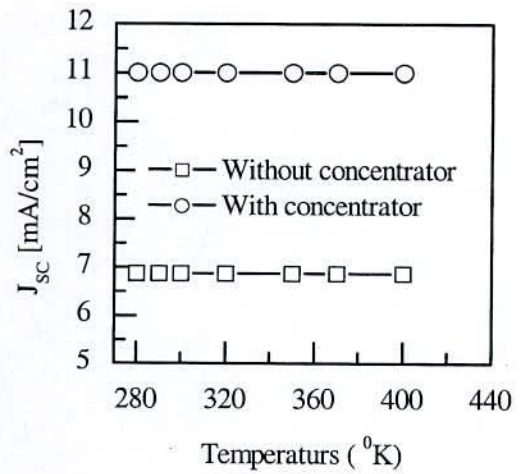
(d) Eight junctions

Fig. 5.5 Variation of short circuit current density, J_{SC}, with temperature in the cells with and without concentrator for 1, 2, 4 and 8 junctions.

(a) Single junction

(b) Two junctions

(c) Four junctions

(a) Eight junctions
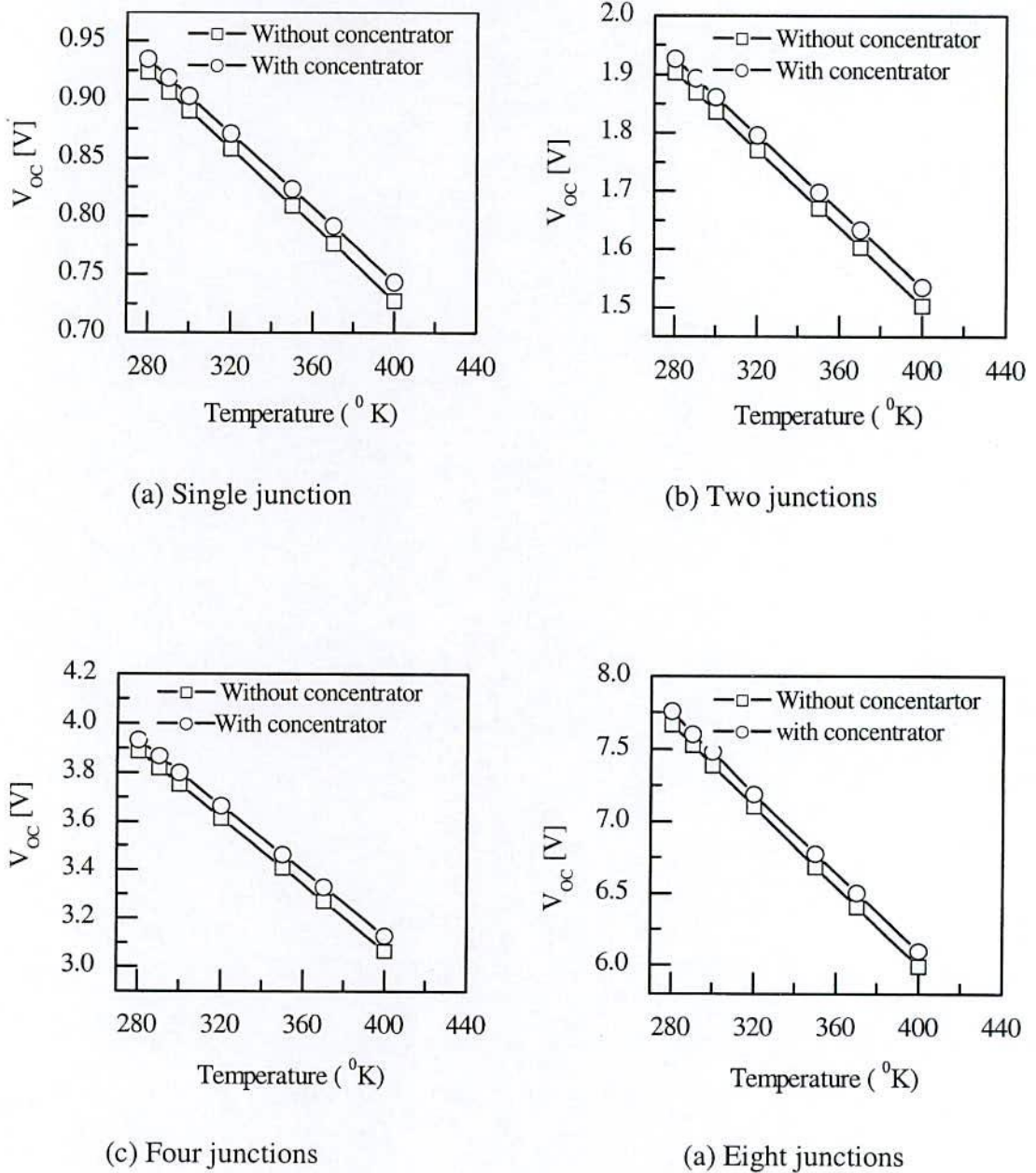
Fig. 5.6 Variation of open circuit voltage with temperature in the cells with and without concentrator for 1, 2, 4 and 8-junctions.

From Eqs. (3.25)– (3.27), it is found that the decrease in V_{OC} with increasing temperature arises mainly from the change in intrinsic carrier concentration (n_i). J_0 increases exponentially with decreasing 1/T, and V_{OC} decreases almost linearly with increasing T.

(a) Single junction

(b) Two junctions

(c) Four junctions

(d) Eight junctions
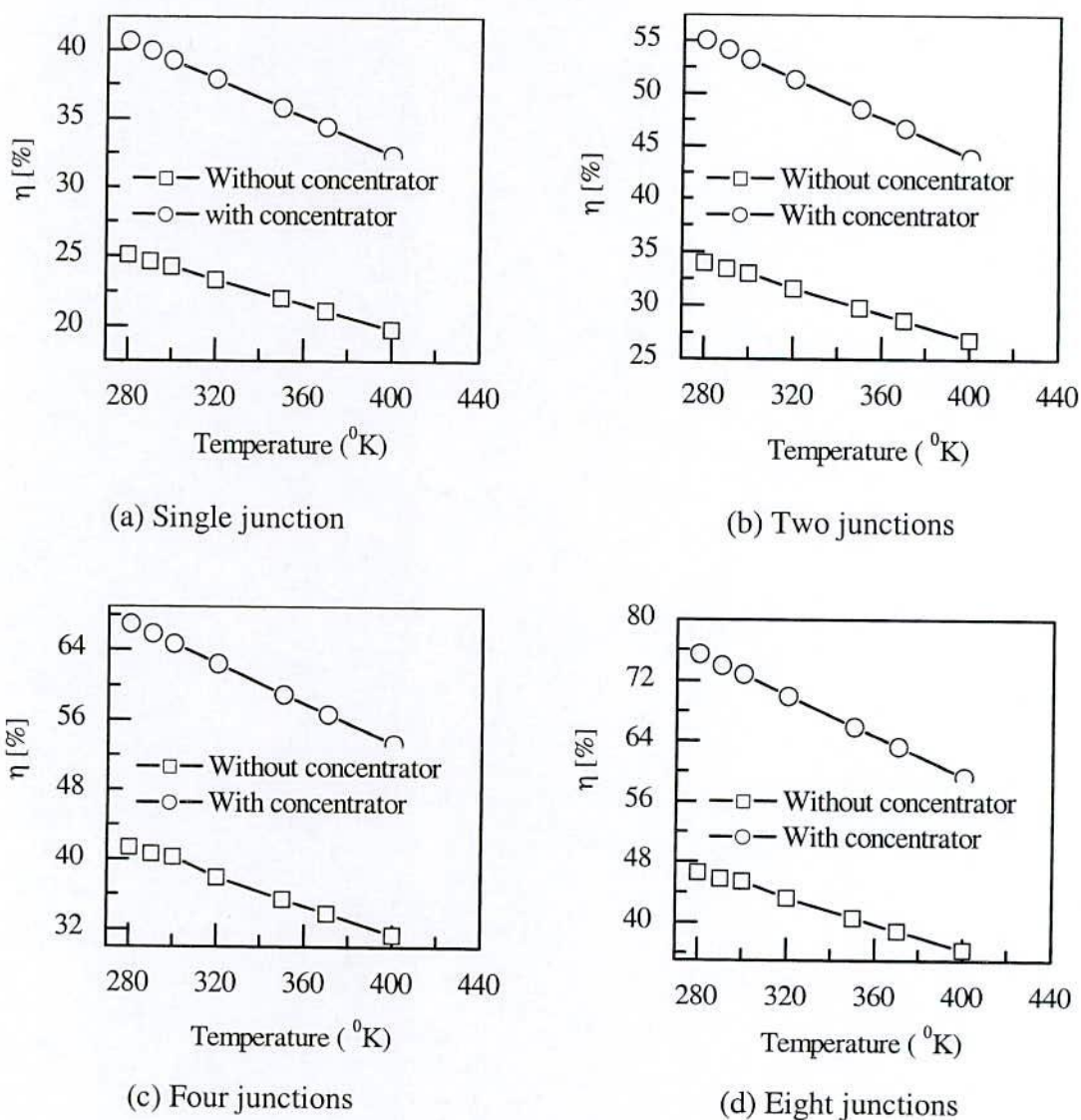
Fig. 5.7 Variation of Efficiency with temperature in the cells with and without concentrator for 1, 2, 4 and 8 junctions.

Figure 4.7 shows the temperature dependence of efficiency. The temperature dependence of efficiency is mostly affected by the temperature dependence of V_{OC}. The calculated temperature dependency results are in good agreement with Nishioka et al. [39]. The effect of temperature on fill factor has not considered during these calculation. Efficiency decreased with increasing temperature, and increased with concentrator. These results indicate that the concentration operations have beneficial effects on InGaN-based multijunction solar cell.

CHAPTER 6
Conclusions and Future Works

6.1 Conclusion

The goal of this work is to study and design of $In_xGa_{1-x}N$-based multijunction solar cells for high performance. In order to realize the high performance $In_xGa_{1-x}N$-based MJ solar cells theoretical design and performance evaluation are very much essential. In this work, we have designed theoretically $In_xGa_{1-x}N$ -based MJ solar cell for high efficiency and predicted the performance. The design and performance evaluation are made by developing a simulation model which optimizes the design of MJ solar cells for high efficiency. The efficiency increases rapidly for first few junctions and then it's increasing tendency becomes slower with increasing junction number. The efficiency evaluated in the present study is found to be varied from 24.49 to 45.35 % for single to eight junction solar cells. The effect of band gap optimization increases the efficiency of $In_xGa_{1-x}N$-based MJ solar cell. But, the effect of band gap optimization on efficiency reduces with the increase of junction number.

There is a significant effect of current and lattice matching on the performance of solar cell. The current of each junction are made equal by adjusting the thickness of the emitter. The current mismatches are kept within 0.29%. The proposed multijunction solar cell is composed of single ternary alloy. The lattice mismatches were found to be varied from a value of 0.86% (minimum) to a value of 3.15% (maximum).

The efficiency of the solar cell is significantly lowered by increasing the surface recombination velocity. The efficiency is found to be varied from 45.35% to 27.72% at recombination velocity 10^3 to 10^6 cm/s, respectively, for eight junctions. The increase in minority carrier lifetime increases the efficiency of the solar cell. The minority carrier lifetime of InN is still unknown but expected to high, thus the variation of efficiency is found to be 45.35% to 46.59% with the increase of minority carrier life time (base diffusion length) from 1.25 to 1.60 μm, respectively, for eight junctions. The effect of emitter thickness on efficiency has been analyzed and found to vary from 46.15% to 35.37% at the thickness $0.2\mu m$ to $0.7\mu m$, respectively. The increase in doping density increases the efficiency which is found about 51 % for eight junctions at carrier concentration 1×10^{20} cm^{-3}.

The efficiency of In$_x$Ga$_{1-x}$N-based multijunction solar cells, under concentration operations, is evaluated. The efficiency with concentrator of each junction is found more than that of without concentrator. The efficiency is found to be varied from 24.49 to 39.28 (%) for single junction and 45.35 to 72.79 (%) for eight junction, without and with concentrator, respectively. The effect of temperature on the performance of the In$_x$Ga$_{1-x}$N-based multijunction solar cells under concentration is also evaluated. The calculated values are found to be in good agreement with the reported values [39]. It is found that the efficiency decreases with increasing temperature.

6.2 Suggestion for Future Works

In the present study a model has been developed to calculate the efficiency of $In_xGa_{1-x}N$-based MJ solar cells with optimized band gap to get the maximum efficiency. The proposed model has been successfully designed with many exciting results. These have created the way for future work with a goal to fabricate practical $In_xGa_{1-x}N$-based high efficiency MJ solar cells. There are many areas where further work is required. The works remaining for future study are discussed as follows.

In this work, the efficiency has been calculated considering the value of some parameters of GaN as $In_xGa_{1-x}N$. As still those parameters are unknown for $In_xGa_{1-x}N$. Using the actual values of the parameters of $In_xGa_{1-x}N$ alloy, the efficiency can be determined more accurately from the model.

The effect of series and shunt resistance has not considered in our calculation. Further work can be extended considering the effect of series and shunt resistance with the help of SPICE software.

The efficiency of solar cell can be further increased using concentrator. Concentrator is a vital component of terrestrial multijunction solar cell systems. The effect of concentrator has been shown for two suns but the variation of concentration ratio has not included in this model. To get the actual result a solar simulator (WACOM, WXS-130S-10T) [42] can be used or other available simulator can be used.

The benefits of piezoelectric effects for photogeneration are reported [40, 41]. By the appropriate use of piezoelectric fields, photogenerated carriers are more efficiently extracted and carrier capture can be prevented. Practical efficiency enhancements are thus projected for piezoelectric structure. Therefore, works can be done to consider the above mentioned effects on the design on InGaN-based MJ solar cells.

Bibliography

[1] J. Wu, W. Walukiewicz, K. M. Yu, W. Shan, J. W. Ager III, E. E. Haller, H. Lu, W. J. Schaff, W. K. Metzger and S. Kurtz, "Superior radiation resistance of $In_{1-x}Ga_xN$ alloys: Full-solar-spectrum photovoltaic material system," *Journal of Applied Physics,* 94, pp. 6477-6482, (2003).

[2] H.L. Cotal, D.R. Lillington, J.H. Ermer, R.R. King, N.H. Karam, "Triple junction solar cell efficiencies above 32%: the promise and systems challenges of their application in high-concentration-ratio pv systems," *Proc. 28th IEEE Photovoltaic Specialists Conf.,* pp.955-960, (2000).

[3] A.W. Bett, F. Dimroth, G. Lange, M. Meusel, R. Beckert, M. Hein, S.V. Riesen and U. Schubert," 30 % Monolithic tandem concentrator solar cells for Concentrations exceeding 1000 suns," *Proc. 28th IEEE Photovoltaic Specialists Conf.,* pp.961-964, (2000).

[4] C.J Gelderloos, C. Assad, P.T. Balcewicz, A.V. Mason, J.S. Powe, T.J. Priest and J.A. Schwartz, "Characterization testing of hughes 702 solar array," *Proc. 28th IEEE Photovoltaic Specialists Conf.,* pp.972-975, (2000).

[5] M.J O'Neill, A.J McDanal, M.F Piszczor, M.I Eskenazi, P.A Jones, C. Carrington, D.L Edwards and H.W Brandhorst, "The stretched lens ultralight concentrator array," *Proc. 28th IEEE Photovoltaic Specialists Conf.,* pp.1135-1138, (2000).

[6] D.D Krut, G.S. Glenn, B. Bailor, M. Takahashi, R.A. Sherif, D.R. Lillington and N.H. Karam, "Wide acceptance angle, non-imaging, triple junction based, 10× composite space concentrator," *Proc. 28th IEEE Photovoltaic Specialists Conf.,* pp.1165-1168, (2000).

[7] J. M. Olson, T. A. Gessert, and M. M. Al-Jasim, *Proceedings 18th IEEE Photovoltaic Specialists Conference,* pp.552, Las Vegas, Oct. 21–25, (1985).

[8] K. A. Bertness, S. R. Kurtz, D. J. Friedman, A. E. Kibbler, C. Kramer, and J. M. Olson, *Appl. Phys. Lett.* 65, pp.989, (1994).

[9] M. Yamaguchi, "Free electron concentration and mobility of InN and In0.68Ga0.32N as a function of displacement damage dose measured by the Hall Effect," Solar Energy Materials & Solar Cells, 75, pp.261, (2003).

[10] C. H. Henry, "Limiting efficiencies of ideal single and multiple energy gap terrestrial solar cells," *Journal of Applied Physics*, 51(8) pp. 4494-4499, August (1980).

[11] Hasna Hamzaoui, Ahmed S. Bouazzi, Bahri Rezig, "Theoretical possibilities of $In_xGa_{1-x}N$ tandem PV structures," *Solar Energy Materials & Solar Cells*, 87 pp. 595-603 Dec. (2005).

[12] P.A. Crossley, G.T. Noel and M. Wolf, "Review and Evaluation of Past Solar Cell Development Efforts" AED R-3346, Contract NASW- 1427, (1968).

[13] C.B. Honsberg, R. Corkish, and S.P. Bremner, "A New Generalized Detailed Balance Formulation to Calculate Solar Cell Efficiency Limits," *Proc. of the 17th European Photovoltaic Solar Energy Conference*, pp. 22-26, (2001).

[14] A. Luque, and A. Martí, "Increasing the Efficiency of Ideal Solar Cells by Photon Induced Transitions at Intermediate Levels," *Physical Review Letters*, vol. 78, pp. 5014–5017, (1997).

[15] M.A. Green, "Limiting Photovoltaics Light Conversion Efficiency," *Progress in Photovoltaics,* 9, pp. 257-261, (2002).

[16] M.A. Green, K. Emery, D.L. King, S. Igari, W. Warta, "Solar cell efficiency tables (version 23)," *Progress in Photovotlaics*, 13, pp. 55-62, (2003).

[17] T. Trupke, M.A. Green, and P. Wurfel, "Improving solar cell efficiencies by up-conversion of sub-band-gap light," *Journal of Applied Physics*, 92, no. 7, pp. 4117-22, (2002).

[18] S. Kolodinski, J.H. Werner, T. Wittchen, and H.J. Queisser, "Quantum efficiencies exceeding unity due to impact ionization in silicon solar cells," *Applied Physics Letters*, 63, no. 17, pp. 2405-7, (1993).

[19] R.D. Schaller, and V.I. Klimov, "High efficiency carrier multiplication in PbSe nanocrystals: implications for solar energy conversion," *Physical Review Letters*, 92, no. 18, pp. 186601/1-4, 2004.

[20] A. Ghani Bhuiyan, Ph D thesis - "ArF Excimer Laser-Assisted Metalorganic Vapor-Phase Epitaxy: A New Approach for Indium Nitride (InN) Semiconductor Growth", University of Fukui, Japan, pp. 2, March (2004).

[21] X. Guo, E.F. Schubert, "Current crowding in GaN/InGaN light emitting diodes on insulating substrates," *Journal of Applied Physics,* 90 (8) pp. 4191-4195, (2001).

[22] R. Hickman, J.M. Van Hove, P.P. Chow, J.J. Klaassen, A.M. Wowchack, C.J. Polley, D.J. King, F. Ren, C.R. Abernathy, S.J. Pearton, K.B. Jung, H. Cho, J.R. La Roche, "GaN PN junction issues and developments," Http://www.mse.ulf.edu /~spear /recent_papers/p-n_junction/pn_junction.pdf, 01/04/2003.

[23] F.Bechstedt, J. Furthmueller, M. Ferhat, L.K. Teles, L.M.R. Scolfaro, J.R. Leite, V.Yu. Davydov, O. Ambacher, R. Goldhahn, "Energy gap and optical properties of $In_xGa_{1-x}N$," *Phys. Status. Solid.* (a) 195 (3) pp. 628-633, (2003).

[24] M. Hori, K.Kano, T. Yamaguchi, Y. Satto, T. Araki, Y. Nanishi, N. Teraguchi, and A. Suzuki, "Optical Properties of $In_xGa_{1-x}N$ with entire alloy composition on InN buffer layer grown by RF-MBE," *Phys. Status. Solid.* (b) 234, (No. 3), pp. 750-754, October, (2002).

[25] M. E. Levinshtein et. al. Properties of advanced semiconductor materials, A wiley-interscience Publication, John wiley & sons, Inc, (2001).

[26] http://rredc.nrel.gov/solar/spectra/am1.5/ on 25/05/06

[27] O. Ambacher et. al. "Pyroelectric properties of Al (In) GaN/GaN hetero and quantum well structure" *J. Phys. Condens Matter* 14, pp. 3399-3434, (2002).

[28] J. W. Ager, W. Walukiewicz, "High efficiency, radiation-hard solar cells", Final report for the Director's Innovation Initiative project DII-2004-593, October 22, (2004).

[29] L. W. James, *Proc. First World Conference on Photovoltaic Energy Conversion,* Hawaii, USA, 1799, (1994).

[30] S. R. Kurtz and M. J. O'Neill, "Estimating and controlling chromatic aberration losses for two-junction, two-terminal devices in refractive concentrator systems," Proc. *25th IEEE Photovoltaic Specialists Conf.,* Washington, D.C., USA, pp. 361-365, (1996).

[31] K. Masuda, Proc. *11th International Photovoltaic Science and Engineering Conference,* 5, (1999).

[32] M. Yamaguichi et al., "Japanese activities of R&D on III-V concentrator solar cells and modules", *Proc. 19th EU-PVSEC,* (2004)

[33] http://sunbird.jrc.it/events/0511fullspectrum/2_1_Yamaguchi.pdf, 25/08/2006

[34] K. Araki, H. Uozumi and M. Yamaguchi, "A simple passive cooling structure and its heat analysis for 500 x concentrator pv module," *Proc. the 29th IEEE Photovoltaic Specialists Conf.,* New Orleans, pp. 1568-1571, (2002).

[35] S. M. Sze, "Physics of Semiconductor Devices", (A WILEY-INTERSCIENCE PUBLICATION), pp. 800-835, (1981).

[36] A. L. Fahrenbruch and R. H. Bube, "Fundamentals of Solar Cells", (ACADEMIC PRESS, INC.), pp. 238-239, (1983).

[37] M. J. O'Neill, A.J. McDanal, A.J. McDanal H.L. Cotal, R. Sudharsanan, D.D. Krut, J.H. Ermer, N.H. Karam, & D.R. Lillington., "Development of terrestrial concentrator modules incorporating high-efficiency multi-junction cells," *Proc. 28th IEEE Photovoltaic Specialists Conf.,* Anchorage, pp. 1161-1164, (2000).

[38] V.D. Rumyantsev, V.M. Andreev, A.W. Bett, F. Dimroth, M. Hein, G. Lange, M.Z. Shvarts, O.V. Sulima, Rumyantsev, "Progress in development of all-glass terrestrial concentrator modules based on composite fresnel lenses and III-V solar cells," *Proc. 28th IEEE Photovoltaic Specialists Conf.,* Anchorage, pp. 1169-1172, (2000).

[39] K. Nishioka et al. *Solar Energy Materials & Solar Cells* 90 pp.57–67, (2006).

[40] Manuel J. Romero and Mowafak M. Al-Jassim, "Advantages of using piezoelectric quantum structures for photovoltaic". *Journal of Applied Physics,* vol. 93, no. 1, pp. 626-631, Jan. (2003).

[41] Sarah Kurtz, J.F. Geisz, D.J. Friedman, A.J. Patk, R.R. King, D.C. Law and N.H. Karam, "Collection of Photocarriers in $Ga_xIn_{1-x}N_yAs_{1-y}$ solar cells". http://www. nrel.gov /docs/fy05osti/37157.pdf on 15/10/2006.

[42] K. Nishioka Ph D thesis "Evaluation and Optimization of Super High Efficiency InGaP/InGaAs/Ge Triple-Junction Solar Cells for Advanced Concentrator Photovoltaic Systems" Nara Institute of Science and Technology, pp. 28, March (2004).

List of Publications

1. **Md. Rafiqul Islam**, M. A. Rayhan, M. E. Hossain, Ashrsful G. Bhuiyan, M. R. Islam, & Akio Yamamoto. "Projected Performance of $In_xGa_{1-x}N$-based multi-junction Solar Cells" Accepted in 4th International Conference on Electrical & Computer Engineering, December 19-21, 2006. Dhaka, Bangladesh, (IEEE catalogue number: 06EX1362).

2. Ashrsful G. Bhuiyan, **Md. Rafiqul Islam**, M. R. Islam, Akihiro Hashimoto & Akio Yamamoto. "Growth and Properties of InN Layer on Sapphire Substrate using LA-MOVPE" Proc. 3rd International Conference on Electrical & Computer Engineering, December 28-30, 2004. Dhaka, Bangladesh (ISBN 984-32-1804-4).

3. M.A. Aziz, **M.R. Islam,** Bhupesh C. Roy & M. Alauddin "Study of Sodium Chlorate Production in a Novel Electrolytic Cell and its Effect on Current Efficiency and power consumption." Journal of Applied Science and Technology, Vol. 02 No. 01 June 2001.

APPENDIX A

Values of Some Parameters

The value of the parameters used in this simulation model.

SL. No	Description of the parameters	Value of the parameters	Unit
01	Reflection Coefficient, R	0.00	-
02	Diffusion length of hole, Lp	0.79	μm
03	Diffusion length of electron, Ln	1.25	μm
04	Surface and the rear recombination velocity, S	1000	cm/s
05	Diffusion coefficient for hole, Dp	9	cm^2/s
06	Diffusion coefficient for electron, Dn	25	cm^2/s
07	Total thickness of the junction	2.00	μm
08	Acceptor atom concentration, N_A	1.00×10^{24}	$/m^3$
09	Donor atom concentration, N_D	1.00×10^{24}	$/m^3$
10	Temperature, T	300.00	K
11	Fill factor, FF	0.85	-
12	Static dielectric constant of GaN ε_r	15.3	
13	Dielectric constant ε_o	8.85×10^{-12}	F/m